Differential roles, crosstalk and response to the Antifungal Protein AfpB in the three Mitogen-Activated Protein Kinases (MAPK) pathways of the citrus postharvest pathogen *Penicillium digitatum*

Mónica Gandía, Sandra Garrigues, Miguel Hernanz-Koers,
Paloma Manzanares, Jose F. Marcos*

Department of Food Biotechnology, Instituto de Agroquímica y Tecnología de Alimentos (IATA), Consejo Superior de Investigaciones Científicas (CSIC), Avda Agustín Escardino 7, 46980 Paterna, Valencia, Spain.

* Corresponding author: Dr. Jose F. Marcos. Instituto de Agroquímica y Tecnología de Alimentos (IATA) - CSIC, Avenida Agustín Escardino 7, Paterna 46980, Valencia, Spain. e-mail: jmarcos@iata.csic.es. Phone: (34)963.900.022. Fax: (34)963.636.301

Abstract

Fungi have three mitogen-activated protein kinases (MAPKs): Kss1/Fus3 involved in the invasive growth and virulence of pathogens, Hog1 in response to osmotic stress, and Slt2/Mpk1 in response to cell wall (CW) stress. We conducted comparative analyses of these MAPKs in the phytopathogen *Penicillium digitatum* and studied their role in the mode of action of the novel self-antifungal protein AfpB. The sensitivity to different stresses of Δ*hog1* and the reduced growth of Δ*kss1* coincided with previous reports. However, Δ*slt2* showed a strong reduction of growth and conidiation, abnormal morphology, and sensitivity to CW stress and temperature. The complementation of Δ*slt2* validated this mutant. Immunodetection of P-Hog1 and P-Slt2 confirmed the loss and gain of MAPKs in the mutant and complemented strains. Mutants Δ*slt2* and Δ*kss1* showed a strong reduction in virulence, whereas Δ*hog1* was the least affected, and none sporulated during infection. We studied the MAPK signalling induction in response to different treatments. Our data revealed a complex crosstalk involving the three MAPKs, the differential responses of Hog1 and Slt2 to various stresses and their induction by AfpB or the fungicide fludioxonil (FD). Δ*hog1* resistance to FD confirmed that Hog1 mediates the activity of FD, whereas Δ*kss1* sensitivity is probably due to the basal activation of Hog1 in Δ*kss1*. None of the three MAPK mutants showed increased sensitivity to AfpB, contrary to previous reports of other antifungal proteins, which indicates that the observed AfpB-mediated activation of Hog1 and Slt2 would not have a defensive role.

Keywords: *Penicillium digitatum*; Postharvest pathology; MAPK signalling; Stress; Antifungal protein.

1. Introduction

Intracellular signalling pathways respond to environmental signals and control growth, development and virulence in phytopathogenic fungi (Turrà et al., 2014; Jiang et al., 2018). Among these pathways, the so-called mitogen activated protein kinase (MAPK) cascades play important roles in fungal biology and involve protein kinases that integrate the response to signals and modulate gene expression through sequential phosphorylation and dephosphorylation cycles (Mehrabi et al., 2012; Hayes et al., 2014). In filamentous fungi there are three MAPK signalling cascades, which are orthologous to the well-characterised five MAPK cascades present in the yeast *Saccharomyces cerevisiae*. The high osmolarity glycerol (HOG) pathway with the Hog1 MAPK protects against hyper-osmotic conditions mediating the accumulation of osmolytes inside the cell; the Slt2 MAPK regulates cell wall integrity (CWI) pathway and responses of CW adaptation; and the Kss1 MAPK controls invasive growth and infection-related morphogenesis (Hamel et al., 2012; Mehrabi et al., 2012; Turrà et al., 2014; Jiang et al., 2018). Depending on each fungus, the three fungal MAPK pathways contribute to the infection of insect, plant, animal or human pathogens in different ways (Roman et al., 2007; Alonso-Monge et al., 2009; Luo et al., 2012; Segorbe et al., 2016; Song et al., 2016). Previous studies also point to the existence of positive or negative overlap between the three pathways, cooperating or establishing crosstalk among them (Hamel et al., 2012; Turrà et al., 2014; Segorbe et al., 2016; Song et al., 2016).

Penicillium digitatum is the main citrus postharvest pathogen. It produces the green mould disease in citrus fruits and is responsible for important economic

losses worldwide (Palou, 2014). Control of citrus postharvest diseases is mainly achieved through treatment with chemical fungicides, which have a negative impact on health and the environment, and result in the development of resistance, reducing their efficacy. Therefore, there is an urgent need to find new control alternatives. Currently, efforts are focused on the discovery and development of new antifungals and the study of the mechanisms that are responsible for pathogenicity and virulence (Gandía et al., 2014; Harries et al., 2015; López-Pérez et al., 2015; Wang et al., 2015; Garrigues et al., 2016; Palou et al., 2016; Vilanova et al., 2016). Among novel antifungal molecules, the use of peptides and proteins has been previously proposed (Marcos et al., 2008; Garrigues et al., 2017a; Garrigues et al., 2017b).

Antifungal proteins (AFPs) are small, cationic, cysteine-rich proteins (CRPs) that are usually secreted in large amounts by filamentous ascomycetes and are specifically active against fungi at micromolar concentrations, which make them good alternatives for the development of novel antifungal compounds (Meyer, 2008; Hegedüs and Marx, 2013). *P. digitatum* encodes only one AFP named AfpB, which was not naturally produced (Garrigues et al., 2016). We have reported the biotechnological production of AfpB in *P. digitatum* (Garrigues et al., 2017b) and, more recently, its transient production in *Nicotiana benthamiana* plants (Shi et al., 2019). The availability of AfpB enabled its characterisation as a highly active antifungal protein that shows potent *in vitro* activity against the self-fungus (Garrigues et al., 2017b) and inhibits infection of tomato by *Botrytis cinerea* (Garrigues et al., 2018).

The three MAPKs have been recently identified and studied in *P*. *digitatum*: The PdOs*2* orthologue of Hog1 (Wang et al., 2014), the PdMpkB orthologue of Kss1

(Ma et al., 2016) and, more recently, PdSlt2 (de Ramón-Carbonell and Sánchez-Torres, 2017). However, in these previous studies each of the three MAPKs has been studied individually in three different strains of *P. digitatum*, which come from different origins and present both genotypic and phenotypic differences. Therefore, these studies lacked comparative analyses to determine the relative effect of each MAPK on the biology of *P. digitatum.* The *PdMpkB* gene was studied in the highly virulent wild-type strain CECT 20796 isolated from an infected orange in Spain (Marcet-Houben et al., 2012); the *PdOs2* in the imazalil-resistant (R1 phenotype) Pd01 strain from China (Sun et al., 2013); and the *PdSlt2* from the thiabendazole- and imazalil-resistant strain Pd1 isolated from grapefruit in Spain (Marcet-Houben et al., 2012). In addition, the two fungicide-resistant strains (Pd1 and Pd01) have better genomic synteny between them than with the wild-type CECT 20796 (Sun et al., 2013).

In an attempt to improve the characterisation and compare the functional roles of the three MAPK pathways in *P. digitatum*, we generated null deletion mutants of the three genes coding for Hog1, Kss1 and Slt2 in the same strain, our wild-type CECT 20796. We found that the Δ*hog1* and Δ*kss1* mutants showed phenotypes very similar to the ones previously reported (Wang et al., 2014; Ma et al., 2016), while Δ*slt2* differed markedly from the previous study on Slt2 (de Ramón-Carbonell and Sánchez-Torres, 2017). We showed that the three MAPK mutants have severe but differential effects on virulence. In addition, we determined the sensitivity of the mutants and the phosphorylation status of the Hog1 and Slt2 MAPKs in response to different treatments including exposure to the fungicide fludioxonil (FD) or the antifungal protein AfpB, whose biological role in the fungus is still unknown (Garrigues et al., 2016; Garrigues et al.,

2017b). Our study reveals important data about the involvement of MAPKs in the mode of action of FD and AfpB, and the crosstalk among the three MAPK pathways that indicate that they act coordinately.

2. Materials and methods

2.1. Strains and culture conditions

Penicillium digitatum CECT 20796 (Marcet-Houben et al., 2012) was used as parental strain. This strain and all transformants generated in this work were cultured on potato dextrose agar (PDA) (Difco 213400) plates for 7-10 days at 25 ºC. For growth analyses, 5 µL of conidial suspension (5 x 10^4 conidia mL^{-1}) of each *P. digitatum* strain were deposited on the centre of PDA or *P. digitatum* minimal medium agar (PdMMA) plates (Sonderegger et al., 2016) and the diameter of growth was measured daily. We determined conidia production as previously described (Gandía et al., 2014). Plasmid vectors were cloned and propagated in *Escherichia coli* JM109 grown in Luria Bertani (LB) medium supplemented with 25 µg mL^{-1} chloramphenicol or 50 µg mL^{-1} kanamycin at 37 ºC. *Agrobacterium tumefaciens* AGL-1 strain was grown in LB medium supplemented by 20 µg mL^{-1} rifampicin at 28 ºC.

Growth in liquid media was evaluated on 96-well microtiter plates (Nunc, Roskilde, Denmark) containing either 5 % potato dextrose broth (PDB) or citrus peel extract (CPE) at 5 x 10^5 conidia mL^{-1} as described (López-García et al., 2002). To prepare orange CPE, frozen orange peel was homogenised with a polytron (1 g in 10 mL of water) and the solution was filtered through Miracloth

and centrifuged at 17,000 x *g* for 10 min. The CPE in the supernatant was sterilised by filtration and stored at -20 ºC.

2.2. Genetic transformation of P. digitatum

For genetic transformation of *P. digitatum*, the *Agrobacterium tumefaciens*-mediated transformation (ATMT) and the dual selection strategy with hygromycin resistance (*hph*) as a positive selection and the Herpes Virus thiamine kinase gene (HSV*tk*) as negative selection markers was used, as described (Khang et al., 2006) with modifications (Harries et al., 2015; Hernanz-Koers et al., 2018). The FungalBraid (FB) modular cloning approach to generate the *hog1* disruption vector was described previously (Hernanz-Koers et al., 2018). The *kss1* and *slt2* genes were disrupted using the same FB strategy. The primers used, the diagrams of the constructs and the confirmatory PCRs are shown in Supp. Table 1 and Supp. Figs. 1 and 2. We assembled FB DNA parts containing: (i) fungal DNA fragments of 1 Kb for *kss1* (primers OJM543 and OJM544 for part FB016, and OJM545 and OJM546 for FB017) or *slt2* disruption (OJM551 and OJM552 for FB020, and OJM553 and OJM554 for FB021) amplified from *P. digitatum* genomic DNA, (ii) the positive selection marker (FB012), and (iii) the Herpes Virus thiamine kinase gene (HSV*tk*) that was used as a negative selection marker (FB013) (Supp. Figs. 1 and 2). The resulting pDGB3α2 vectors (FB023 for *kss1* and FB025 for *slt2*) were transformed into *A. tumefaciens* AGL-1 strain and used in the fungal transformation of the parental CECT 20796 (Harries et al., 2015). Homologous recombinants were confirmed by PCR amplification of genomic DNA with

147 discriminatory primers (Supp. Figs. 1 and 2), as previously described (Gandía et
148 al., 2014) .

149 For genetic complementation, we introduced a wild-type functional copy of *slt2*
150 gene into a Δ*slt2* mutant. One fragment of 2.7 kb (including the native promoter,
151 coding sequence and terminator) was amplified from *P. digitatum* genomic DNA
152 with primers OJM574/OJM575 (Supp. Table 1), and cloned into the pGEM-T
153 vector (Promega). The resulting insert was digested with *Xba*I and *Hin*dIII
154 restriction enzymes and introduced into the newly described pCnptII vector
155 (Supp. Fig. 3), which confers geneticin resistance. The resulting
156 complementation vector (pCnptII_Slt2) was used for ATMT of the Δ*slt2* mutant.
157 Positive transformants were selected for geneticin resistance (25 μg mL^{-1}) and
158 confirmed by PCR amplification of genomic DNA.

159 *2.3. Phenotypic characterisation of transformants*

160 For the phenotypic characterisation, 5 μL of serial 10-fold dilution of conidia (10^5
161 to 10^3 conidia mL^{-1}) were applied into PDA 24-well plates supplemented with
162 different compounds (Gandía et al., 2014): 150 μg mL^{-1} calcofluor white (CFW),
163 150 μg mL^{-1} congo red (CR), 0.5 M sodium chloride (NaCl), or 1.2 M sorbitol.
164 Sensitivity to temperature was tested by incubating plates at 28 ºC. Fungicide
165 treatment was performed in PDA supplemented with different concentrations of
166 thiabendazol (TBZ) (0.5 and 1 μM), imazalil (IMZ), (0.0625 and 0.125 μM),
167 fludioxonil (FD) (0.2 and 0.4 μg mL^{-1}) and iprodione (IPD) (2 and 4 μg mL^{-1}).

2.4. Sensitivity to the antifungal protein AfpB

Growth inhibition assays were performed in 96-well microtiter plates as described (Garrigues et al., 2017b) with minor modifications. A volume of 50 µL of fungal conidia (5×10^4 conidia mL^{-1}) in 1/10 diluted PDB medium containing 0.02% (w/v) chloramphenicol, was mixed in each well with 50 µL of 2x concentrated AfpB solution from serial two-fold dilutions (from 0.25 to 8 µg mL^{-1}). Plates were statically incubated for 7 days at 25 ºC, and growth was determined daily by measuring the optical density (OD) at 600 nm. Low magnification images of each well in the plate were visualised under the microscope (E90i, Nikon Chiyoda, TO, Japan), captured by the NIS-Elements BR v2.3 software (Nikon) and processed by the FIJI software (Schindelin et al., 2012).

2.5. Microscopy

Sample preparation, fixation, staining using CFW, and microscopic visualisation (E90i microscope, Nikon Chiyoda, TO, Japan) were conducted as previously described (Garrigues et al., 2016). Bright fields and fluorescence images were captured by the NIS-Elements BR v2.3 software (Nikon) and processed using FIJI software (Schindelin et al., 2012).

2.6. Fruit infection assays

Fruit infection assays on mature freshly harvested oranges (*Citrus sinensis* L. Osbeck cv Navelina) or mandarins (*Citrus reticulata* cv. Clemenules) were conducted as described (González-Candelas et al., 2010). Three replicates of five fruits were inoculated at four wounds around the equator with 5 µL of

191 conidial suspensions (5 x 10^4 conidia mL^{-1}). Each inoculated wound was scored
192 for symptoms at different days post-inoculation (dpi), and the mean and
193 standard deviation (SD) of the percentage of infected wounds calculated.

194 *2.7. Western analyses*

195 Suspensions of 2 x 10^6 conidia mL^{-1} of the *P. digitatum* strains were grown in
196 100 % PDB at 25 ºC and 80 rpm for 24 h. To evaluate the response to different
197 treatments, 24 hours-old mycelium of CECT 20796 was exposed to H_2O as
198 control treatment, 0.5 M NaCl, 150 µg mL^{-1} CFW, 150 µg mL^{-1} CR, 0.05 µg mL^{-1}
199 FD or 10 µg mL^{-1} AfpB, for 20 and 60 min. Mycelia were filtered, dried and
200 ground in liquid nitrogen. Proteins were extracted in a ratio 1:2 (w/v) of ground
201 mycelium to the protein extraction buffer described previously (Yang et al.,
202 2013) with modifications [187.5 mM Tris–HCl pH 8.8, 10 % glycerol, 2 %
203 sodium dodecyl sulfate (SDS), 10 mM dithiothreitol, 1mM sodium
204 orthovanadate, 1mM phenylmethylsulfonyl fluoride (PMSF) (Sigma-Aldrich, St
205 Louis, MO, USA), 1X phosphatase inhibitor (Thermo-Fisher, Waltham, MA,
206 USA), 10 mM β-mercaptoethanol, 5 µL protease inhibitor cocktail (Sigma-
207 Aldrich)]. The homogenate was transferred to 2 mL tubes, vortexed three times,
208 and centrifuged at 12000 x *g* for 10 min. The proteins in the supernatant were
209 separated on 10 % denaturing polyacrylamide gel (SDS-PAGE), transferred to
210 Optitran BA-S 85 0.45 µm nitrocellulose membrane (Schleicher and Schuell,
211 Dassell, Germany) and immunodetected essentially as described (Torres-
212 Quiroz et al., 2010). Phosphorylated P-Hog1 and P-Slt2 were detected with
213 phospho-p38 MAPK (#9211S, Cell signalling Technology) and phospho-p44/42
214 MAPK (Thr202/Tyr204) (#4370, Cell signalling Technology) antibodies. Actin as

215 loading control was detected with anti-actin antibody (Sigma-Aldrich). Complete
216 western membranes are shown in Supp. Fig. 4.

217 **3. Results**

218 *3.1. Identification of MAPK Slt2 and Hog1 in the P. digitatum strain CECT*
219 *20796.*

220 In previous studies, the MpkB MAPK (accession ID EKV07229/PDIG_75030)
221 was identified and characterised in the Spanish wild-type *P. digitatum* CECT
222 20796 (Marcet-Houben et al., 2012) as a protein homologous to the MAPK
223 Fus3 of yeast and Kss1of fungi (Ma et al., 2016). In this study, we have used
224 the Kss1 nomenclature for this gene (Turrà et al., 2014). We identified the other
225 two MAPKs in this genome as Hog1 (PDIG_79560) and Slt2 (PDIG_73290),
226 with 99.5 % and 100 % identity to Os2 from Pd01 (Wang et al., 2014) and Slt2
227 from Pd1 (de Ramón-Carbonell and Sánchez-Torres, 2017), respectively. Both
228 proteins are within the Hog1 and Slt2 cluster, as demonstrated by phylogenetic
229 analysis (Supp. Fig. 5).

230 *3.2. Generation of kss1 and slt2 null mutants and slt2 complementation strains.*
231 Recently, we presented the FungalBraid (FB) modular cloning technology
232 (Hernanz-Koers et al., 2018), and we used it to assemble constructs for gene
233 deletion by homologous recombination using dual (positive and negative)
234 selection. We then exemplified the FB strategy with the generation of *hog1*
235 disruption strains. In this work, we used FB to obtain the vectors FB023 and
236 FB025 to disrupt *kss1* and *slt2*, respectively, by assembling the universal DNA
237 modules FB012 (positive *hph* marker) and FB013 (negative HSV*tk* marker) to 1
238 kb flanking fragments located at 5´and 3´ of each selected locus (Supp. Fig. 1A

239 and Supp. Fig. 2A). DNA modules were assembled into the pDGB3α2 binary
240 vector to obtain plasmid vectors FB023 and FB025, which were used for ATMT
241 of *P. digitatum* CECT 20796.
242 Monosporic independent transformants were confirmed by PCR amplification of
243 genomic DNA using primers to discriminate positive null mutants from negative
244 ectopic insertions or wild-type genotypes (Supp. Fig. 1B and Supp. Fig. 2C).
245 Further studies were conducted with two independent strains for each null
246 mutant: strains PDMG5212 and PDMG5241 for Δ*kss1*; PDMG5422 and
247 PDMG5431 for Δ*slt2*; and PDMG5121 and PDMG5135 for Δ*hog1*.
248 Preliminary characterisation of our Δ*hog1* and Δ*kss1* mutants in axenic growth
249 did not reveal substantial differences with the mutants previously reported
250 (Wang et al., 2014; Ma et al., 2016). On the contrary, our Δ*slt2* strains showed a
251 clear restriction of growth and a reduction of conidiation during axenic culture
252 (see Figs. 1 and 2) that was not observed in the previously reported *Pdstl2*
253 mutant in Pd1 strain (de Ramón-Carbonell and Sánchez-Torres, 2017). Since
254 this previous work lacked a complementation control, we decided to obtain a
255 complemented strain of our Δ*slt2* mutant. A copy of the *slt2* gene with its own 5'
256 (promoter) and 3' (terminator) flanking regions was reintroduced into the
257 PDMG5431 (Δ*slt2*) strain (Supp. Fig. 2B). The resulting PDMG6134 strain was
258 resistant to both hygromycin used for gene knockout and geneticin used for
259 gene complementation, confirming the integration of the complementation
260 construct. All the subsequent characterisation assays confirmed that the
261 complemented PDMG6134 behaved like the wild-type strain and, therefore, had
262 integrated a functional copy of the *slt2* gene.

3.3. Elimination of the slt2 gene strongly affects growth and conidiation of P. digitatum

The growth of the different strains in distinct media was analysed side by side to compare the relative role of MAPKs. First, the growth rate and morphology was determined on rich PDA and on PdMMA plates (Fig. 1A-C). The Δ*hog1* mutants showed no significant difference in their growth rate compared to the wild-type strain on both media, although irregular shape in the contour of these colonies was noticeable. (Fig. 1A). On the other hand, the Δ*kss1* and Δ*slt2* mutants presented slower growth rates than wild-type, and this difference in growth was more pronounced in PDA than in PdMMA (Fig. 1B and 1C). The Δ*kss1* mutants exhibited a characteristic irregular shape in PDA and were more affected in PdMMA, whereas Δ*slt2* mutants were more affected in rich PDA medium. The complemented strain PDMG6134 (Δ*slt2*::*slt2*), displayed a normal growth rate similar to that of CECT 20796 on both media (Fig. 1A-C). We also determined the growth of all strains in liquid PDB medium (Fig. 1D) and in CPE from oranges (Fig. 1E), trying to emulate the substrates that the fungus will encounter in its natural niche. Under these conditions, the Δ*slt2* mutants showed an initial delay in their growth capability, similar to the observations in solid medium. However, both parental and Δ*slt2* mutant strains reached similar OD, and therefore, similar growth, at later time points. All these results indicate that (i) *hog1* is not required for normal mycelial growth, and (ii) the deletion of *kss1* and *slt2* affects *P. digitatum* growth in a very different manner.

Next, we quantified the conidia production in all the mutant strains generated in this work. Only in the case of the Δ*slt2* mutant the amount of conidia was significantly reduced up to 75 % compared to CECT 20796, and this amount

288 was completely restored in the complemented strain (Fig. 2A). We therefore
289 studied the conidiogenesis of Δ*slt2* in more detail. Fluorescence microscopy
290 after CFW staining was consistent with conidia quantification. After 48 h of
291 growth, the wild-type CECT 20796 (Fig. 2B) and the complemented strain
292 PDMG6134 (data not shown) presented normal conidiophores with strings of
293 conidia; however, in PDMG5431 (Δ*slt2*) the conidiophores were rare (Fig. 2B).
294 At this time, the mutant showed balloon-like structures similar to those observed
295 in chitin synthase mutants (Gandía et al., 2014), indicating an altered CW. After
296 72 h of growth, the wild-type and complemented strains produced long conidial
297 chains (Fig. 2C), while the mutant had enlarged hyphae tips that suggest
298 aborted conidiophores. These results denote the important role of *slt2* gene in
299 *P. digitatum* growth, development and conidia production.

300 *3.4. Differential involvement of the MAPK from P. digitatum in response to*
301 *stress and sensitivity to chemical fungicides.*

302 Mutant strains in the *hog1* gene showed increased sensitivity to osmotic stress
303 caused by NaCl or sorbitol (Fig. 3A). These mutants did not show different
304 growth on CFW or CR, which are compounds that target the CW, but they had a
305 slightly reduced growth at high (28 ºC) temperatures (Supp. Fig. 6). In contrast,
306 the growth defect of Δ*slt2* mutants was partly recovered in the presence of NaCl
307 or sorbitol (Fig. 3A), showing an inverse effect to that of Δ*hog1* strains. The
308 growth of Δ*slt2* was completely inhibited in presence of CFW, CR, or at high
309 temperatures, indicating important CW alterations (Fig. 3B) and showing the
310 contribution of this MAPK pathway to maintain CWI. Conversely, Δ*kss1* mutants
311 did not show any differential behaviour compared to parental strain growing in

PDA supplemented with NaCl, sorbitol, CFW, CR or at high temperatures (Fig. 3A and Supp. Fig. 6).

Currently, treatment of citrus postharvest diseases includes the use of fungicides with different modes of action such as TBZ, which blocks microtubule assembly, or IMZ, which inhibits ergosterol biosynthesis (Palou, 2014). Other fungicides that are not so frequently used are the FD, which inhibits transport-associated phosphorylation of glucose, and the IPD, which inhibits the germination of fungal spores. These latter ones were suggested to interfere with the osmosensing signal transduction pathway (Pillonel and Meyer, 1997). The MAPK mutants were grown in presence of different concentrations of these four fungicides. Analyses of resistance showed that TBZ and IMZ did not have significant effects on the mutant strains compared to the parental strain (Supp. Fig. 7). Assays with FD and IPD showed differential behaviour in the mutant strains (Fig. 3C). The Δ*hog1* strains presented increased resistance to FD whereas Δ*kss1* and Δ*slt2* were more susceptible. Only Δ*slt2* showed increased sensitivity to IPD, while the other strains did not exhibit significant growth differences to IPD (Fig. 3C).

3.5. The three MAPK cascades are required for virulence of P. digitatum.

The involvement of different *P. digitatum* MAPK pathways in pathogenesis was studied by comparing the virulence of the different mutants to orange or mandarin fruits (Fig. 4). Mandarins are more sensitive to infection than oranges and show a quicker development and higher incidence of infection in parallel inoculation experiments with the same inoculum dose (Fig. 4A-B).

In oranges, the development, incidence of infection and symptom severity were significantly reduced in all mutants compared to the parental and the *slt2*

complemented strains (Fig. 4A). The Δ*kss1* and Δ*slt2* mutants showed a more pronounced delay and reduction of incidence than Δ*hog1*. At this inoculum dose, only parental and complemented strains developed sporulated mycelium that covered the fruits (Fig. 4C). MAPK mutants produced maceration on oranges around the inoculation site in the few wounds that became infected (5-10 %) that only in case of Δ*hog1* showed areas of fungal white mycelium (Fig. 4C).

In the more susceptible mandarins, the symptoms appeared earlier than in oranges and the incidence of infection was similar in parental, complemented and Δ*hog1* strains. The percentage of infected wounds in Δ*kss1* and Δ*slt2* mutants was similar between them and lower than in the rest of strains (Fig. 4B). Sporulated wounds only appeared in the fruits that were infected by parental and complemented strains, whereas the Δ*hog1* strain produced tissue maceration and developed white fungal mycelium in all inoculated wounds that covered the entire fruit surface, although this white mycelium did not develop into sporulated areas even at late time points. The Δ*kss1* and Δ*slt2* mutants only generated macerated areas without mycelium presence (Fig. 4D). It is important to note that in the wounds infected with the Δ*slt2* mutant, the maceration area progressed more slowly than in those infected with the other strains and, over time, maceration turned into a dark area around the lesion, showing signs of tissue necrosis (Fig. 4D) that completely stopped the progression of maceration, as it was evident at later times (Fig. 4E).

3.6. Induction of Hog1 and Slt2 pathways in response to osmotic and CW stresses and fungicides

To check the phosphorylation status of the different MAPKs in all strains, we tested different commercial phospho-MAPK specific antibodies by western-blot

362 analyses. Only antibodies against phosphorylated p38 MAPK and
363 phosphorylated p44/42 MAPK gave positive and reliable results that were
364 sustained by the appearance/disappearance of immunoreactive bands in the
365 different strains (Fig. 5A). The phosphorylated p38 MAPK antibody gave two
366 immunoreactive bands in the parental strain (Fig. 5A), the lower one being more
367 intense than the upper. The Δ*hog1* mutant selectively lost the lower band that
368 was therefore attributed to the P-Hog1 protein. The single immunoreactive band
369 detected with the phosphorylated p42/44 MAPK antibody in the parental strain
370 disappeared in the Δ*slt2* mutant, and was recovered in the complemented
371 Δ*slt2::slt2* strain (Fig. 5A), confirming its identity as P-Slt2. In addition,
372 comparison of the results with both antibodies among the different strains
373 indicated that the faint upper band detected by the anti P-p38 corresponds to
374 cross reaction with P-Slt2. These results further confirmed the correct deletion
375 of both genes and the complementation of Δ*slt2*. Interestingly, western analysis
376 also showed that basal phosphorylation of Hog1 was increased in the Δ*slt2*
377 mutant. We could not detect P-Kss1 in our experiments because none of the
378 antibodies tested gave reliable results. However, the analysis of the
379 corresponding Δ*kss1* mutant demonstrated a high level of basal
380 phosphorylation of both P-Hog1 and P-Slt2. Quantification and normalisation of
381 the immunoreactive signals demonstrated a 12-fold and 21-fold increase of
382 basal P-Hog1 in the Δ*slt2* and Δ*kss1* mutants, respectively, and a 4 to 5-fold
383 increase of basal P-Slt2 in the Δ*kss1* mutant (Fig. 5C).
384 The following experiments determined the induction of the Hog1 and Slt2
385 pathways in the parental strain CECT 20796 in response to sub-lethal
386 treatments of NaCl (0.5 M), CFW (150 μg mL^{-1}), CR (150 μg mL^{-1}), or FD (0.05

387 μg mL^{-1}) (Fig. 5B). Results showed a quick phosphorylation of the Hog1 protein
388 after exposure to NaCl, CFW and CR for 20 min. This response was not
389 maintained over time and phosphorylation levels dropped at 60 min, revealing
390 an early and sharp response to these compounds. Exposure to FD induced a
391 quick Hog1 phosphorylation at 20 min that was maintained at 60 min of
392 fungicide treatment (Fig. 5B and 5D). A similar pattern was observed with the
393 phosphorylation of the Slt2 protein by CFW, CR and FD. Interestingly, osmotic
394 stress by NaCl treatment repressed Slt2 phosphorylation, thus showing a
395 differential response with the above treatments.

396 *3.7. The MAPK pathways respond to and mediate the mode of action of the*
397 *antifungal protein AfpB*

398 The antifungal protein AfpB is highly active against many filamentous fungi
399 including the fungus *P. digitatum* from which the gene was identified, with a
400 minimum inhibitory concentration (MIC) of 4 μg mL^{-1} (Garrigues et al., 2017b).
401 However, the role of AfpB in the biology of *P. digitatum* remains unsolved
402 despite the generation of null Δ*afpB* mutants and overproducer strains
403 (Garrigues et al., 2016; Garrigues et al., 2017b).
404 The exposure of mycelium of *P. digitatum* to 10 μg mL^{-1} AfpB produced a
405 gradual increase of Hog1 and Slt2 phosphorylation from 20 min to 60 min (Fig
406 6A and 6B). The kinetics of MAPK phosphorylation was thus similar to that
407 observed with the fungicide FD and reached the highest levels of
408 phosphorylation of all the treatments tested for both MAPKs in our study.
409 Therefore, we decided to test whether any of the MAPK mutants behaved
410 differently regarding their sensitivity to AfpB by determining dose-response
411 curves of growth inhibition. In the experiment shown in Fig. 6C, the MIC value of

412 the parental strain determined by OD measurement was 2 μg mL^{-1}. OD
413 measurements showed a slight increase of tolerance in mutants Δ*hog1* and
414 Δ*slt2* (Fig. 6C). Microscopic visualisation of the wells showed patches of
415 abnormal mycelial growth in the three mutants in presence of AfpB at 2 μg mL^{-1},
416 wherein no growth was observed in the parental strain (Fig. 6D). We even
417 observed clearly distinguishable hyphae in the mutant Δ*hog1* at 4 μg mL^{-1} of
418 AfpB.

419 **4. Discussion**

420 There are reports of the differential function of MAPKs in infection and in
421 virulence of fungal phytopathogens (Zheng et al., 2012; Segorbe et al., 2016;
422 Pareek and Rajam, 2017; Sakulkoo et al., 2018). Most of these studies were
423 presented gene-by-gene and/or carried out in different strains of the same
424 fungus and, therefore, it is difficult to draw solid conclusions regarding the
425 relative importance of different MAPKs. This is the case of *P. digitatum*, in which
426 each of the three MAPKs were mutated in a different strain and presented
427 individually (Wang et al., 2014; Ma et al., 2016; de Ramón-Carbonell and
428 Sánchez-Torres, 2017). Through the generation of *P. digitatum* null mutants in
429 the three MAPKs within the same study and strain, our work establishes the
430 possible interconnections among the three MAPK routes in the biology of the
431 *P. digitatum* from its axenic growth to its virulence, and provides data on the
432 cooperative roles in response to different stresses.

433 Our results confirm the involvement of *hog1*/*os2* (Wang et al., 2014) and
434 *kss1*/*mpkB* (Ma et al., 2016) in the growth and response to stress in
435 *P. digitatum*. The *P. digitatum* Δ*hog1*/*os2* mutant showed no phenotypic effect

436 during axenic growth but important growth defects under osmotic stress (Figs. 1
437 and 3). Our data showed that Δ*kss1* had an intermediate growth capability
438 between the Δ*hog1* and the Δ*slt2* mutants (Fig. 1), and colonies had a marked
439 irregular shape already observed for Δ*kss1*/*mpkB* (Ma et al., 2016).

440 The previous *Pdslt2* null mutant obtained in the *P. digitatum* Pd1 strain had
441 identical morphology and sporulation to the parental Pd1 during axenic culture,
442 and defects in sporulation were only reported during fruit infection (de Ramón-
443 Carbonell and Sánchez-Torres, 2017). This previous study did not report other
444 phenotypes related to CW (i.e., sensitivity to CFW or CR) or fungicides. The
445 *P. digitatum* Δ*slt2* strains presented here have important defects in axenic
446 growth (Fig. 1), reduction of conidia production that correlated with defects in
447 conidiophore development (Fig. 2), enlarged balloon-like cells in hyphae (Fig. 2)
448 and increased sensitivity to CW altering compounds (CFW and CR) and
449 temperature (Fig. 3). Observations similar to ours have been reported for *slt2*
450 mutants in other fungi such as *B. cinerea* (Rui and Hahn, 2007) or *Fusarium*
451 *oxysporum* (Segorbe et al., 2016). These phenotypes are consistent with a role
452 of Slt2 in CWI and response to CW stress. It remains to be determined the
453 reasons for the discrepancies between ours and the previous study. Our data
454 were validated with the disappearance of the corresponding P-Slt2 protein in
455 the mutant and its restoration in the complemented strain. Other authors have
456 described phenotypic variations in mutants of the same gene obtained in
457 different parental strains of the same fungus *B. cinerea* (Siewers et al., 2005;
458 Liu et al., 2008).

Our side-by-side approach permitted novel conclusions on the relative importance of the three MAPKs in *P. digitatum* virulence (Fig. 4). The virulence of all the three MAPK mutants was severely affected in fruit, being the Δ*hog1* mutant the least affected and Δ*kss1* and Δ*slt2* similarly affected in terms of incidence. However, the Δ*slt2* mutant failed to fully expand from the inoculated point to the full surface of mandarins (Fig. 4D), probably as consequence of its slow growth and CW defects. The relative importance of the three MAPKs in *P*. *digitatum* is, therefore, different from *F*. *oxysporum*, for which Fmk1/Kss1 was absolutely essential for pathogenesis in tomato plants while Δ*mpk1*/*slt2* and Δ*hog1* mutants showed a partial decrease of virulence that was more pronounced in Δ*mpk1*/*slt2* (Segorbe et al., 2016). Hence, the relative importance of the three MAPKs for pathogenesis differs in different fungi. None of our three mutants was able to sporulate on the fruit surface and only the Δ*hog1* could develop significant white mycelium areas over mandarins. The previous *hog1*/*os2* (Wang et al., 2014) or *kss1*/*mpkB* (Ma et al., 2016) deletants of *P. digitatum* showed smaller macerated lesions than the ones caused by the parental strain, but no reduction of incidence was reported, likely due to the much higher inoculum dose compared to our study (5 x 10^6 versus 5 x 10^4 conidia mL^{-1}). The reduced virulence of the three mutants does not seem to be explained by increased susceptibility to water-soluble citrus molecules, as all of them reached high OD after growth on orange CPE, although growth of Δ*slt2* was retarded (Fig. 1).

Importantly, *hog1* deletion does not affect pathogenesis the same way in different fungi, suggesting that this pathway plays a species-specific role in pathogenesis (Turrà et al., 2014; Jiang et al., 2018). In *Fusarium graminearum*

(Nguyen et al., 2012; Zheng et al., 2012) or *B. cinerea* (Segmuller et al., 2007) the Hog1 pathway seems to be involved in virulence, whereas in other fungi such as *Magnaporthe oryzae*, *hog1* mutants are fully pathogenic (Dixon et al., 1999). On the other hand, the involvement of Kss1/Fus3 in virulence is almost universal and has been demonstrated in many phytopathogenic fungi as *F. oxysporum* (Di Pietro et al., 2001), *Colletotrichum lagenarium* (Takano et al., 2000), or *B. cinerea* (Zheng et al., 2000). Likewise, *P. digitatum* mutants of the Ste12 transcription factor, which is downstream of Kss1, showed a reduction of virulence to citrus fruits measured as macerated area (Vilanova et al., 2016). It is assumed that the main contribution of Kss1 to virulence relates to its role in infection-specific morphogenesis, invasive growth and host penetration (Rispail et al., 2009; He et al., 2017). Recently, the involvement of Kss1/Pmk1 has been demonstrated in rice cell-to-cell invasion and deployment of different effectors to abolish plant immunity in *M. oryzae* (Sakulkoo et al., 2018). However, *P. digitatum* is a necrotroph that does not form specific infection structures but requires pre-existing wounded tissue to infect. We conducted *in vitro* invasive growth assays as described (Rispail et al., 2009; Harries et al., 2015; He et al., 2017), which unexpectedly did not result in conclusive data and indicated that invasive growth was not affected in our *P. digitatum* Δ*kss1*.

It is important to note the dark macerated areas in mandarin fruits infected by the Δ*slt2* mutant (Fig. 4E), despite the high susceptibility of mandarins. These necrotic areas did not progress further and the maceration and infection stopped. This behaviour is similar to that observed in the PDMG152 strain that constitutively expresses the *afpB* gene (Garrigues et al., 2016), and could be a mixed consequence of slow-growing phenotype of the Δ*slt2* mutant and its

509 inability to respond to plant defences. Experimental treatments that induce fruit
510 resistance to *P. digitatum* also restrict infection around the inoculation site
511 (Ballester et al., 2011). In *M. oryzae*, the Mps1 MAPK homologous to Slt2 is
512 involved in plant infection, and the inactivation of *mps1* caused restriction of
513 infection at the penetration point (Zhang et al., 2017). It has been proposed that
514 fungal and plant MAPKs interplay during the plant-pathogen interaction and that
515 pathogenesis-related processes controlled by fungal MAPKs led to the
516 modulation of host defence by plant MAPKs (Hamel et al., 2012). Therefore, it
517 could be that the inactivation of *P. digitatum* MAPKs (for instance Slt2) results in
518 the unbalance of this interplay and thus enhancement of citrus fruit defence
519 responses.

520 The Western blot analyses performed in this work allowed the confirmation of
521 the mutants obtained, and were used to establish an interconnection model
522 among the different MAPK cascades in *P. digitatum* (Fig. 7). The Hog1 pathway
523 appears as a central hub of the MAPK-mediated responses in *P. digitatum*,
524 since Hog1 was induced in all the stress conditions and treatments tested in our
525 study, and its induction by CW stresses (CFW or CR) was even more intense
526 than that of the canonical CWI pathway of Slt2 (Figs. 5D and 7). Cooperation
527 between Hog1 and Slt2 cascades in the response to CW damage has been
528 reported in filamentous fungi and yeast (García-Rodriguez et al., 2000;
529 Rodríguez-Peña et al., 2005; Segorbe et al., 2016; Song et al., 2016), and our
530 data underline the importance of the Hog1 response to CW damage. The Hog1
531 pathway regulates the expression of chitin synthase genes in yeast (Munro et
532 al., 2007). Our *P. digitatum* Δ*slt2* mutant has altered CW (Fig. 3), a basal
533 activation of the Hog1 cascade (Fig. 5), and abnormal structural similar to chitin

534 synthase mutants (Fig. 2), and therefore it seems probable that expression of
535 chitin synthases is also altered, although further studies are needed to confirm
536 this assumption. In addition, Hog1 was especially activated in the *P. digitatum*
537 Δ*kss1*mutant. Conversely, the Δ*hog1* mutant did not show differences in the
538 basal activation of Slt2 (Figs. 5), revealing interactions and non-reciprocal
539 negative regulations for which Hog1 plays a pivotal role (Fig. 7).

540 The differential kinetics and timing of Hog1/Slt2 induction or repression was
541 also significant, and was different in the osmotic (NaCl), CW (CFW or CR),
542 fungicide (FD) or AfpB protein stresses. The activation of the Hog1 pathway
543 upon NaCl, CFW or CR addition is a fast response that occurred at short times
544 (20 min) and decayed at long times (60 min). Similar results were observed
545 when *Beauberia bassiana* was exposed to osmotic stress (Liu et al., 2017). In
546 addition, osmotic stress (NaCl) repressed drastically the phosphorylation of
547 Slt2. On the contrary, the Hog1/Slt2 activation by FD or AfpB was more
548 sustained in time, which is an indication that this activation is not part of a
549 defence response but of the mode of action of either FD or AfpB.

550 Phenylpyrrole fungicides such as FD result in the stimulation of the synthesis of
551 glycerol and mannitol, whose intracellular accumulation is associated with the
552 osmotic stress response (Zhang et al., 2002). FD produces the hyperactivation
553 of the Hog1 MAPK pathway required for the sensitivity to this fungicide
554 (Segmuller et al., 2007; Hayes et al., 2014). This has been previously shown for
555 *P. digitatum* by the genetic and molecular characterisation of natural FD
556 resistant isolates (Kanetis et al., 2008) and the increased resistance to FD of
557 Δ*hog1* null mutants (Wang et al., 2014). Other Δ*hog1* mutants were resistant to

FD in *Neurospora crassa* (Zhang et al., 2002), *F. graminearum* (Nguyen et al., 2012), or *M. oryzae* (Motoyama et al., 2008). Our Δ*hog1* mutants were also more tolerant to FD (Fig. 3C). The western assays confirmed the activation of the Hog1 MAPK by FD treatment (Fig. 5), as previously described in *P. digitatum* (Kanetis et al., 2008), but in a kinetics that was sustained up to 60 min, and different to that of CW or osmotic stresses, which could contribute to explain the deleterious effect of the fungicide. We also demonstrated the coordinated induction of the Slt2 MAPK by FD, although with lower intensity than Hog1 (Fig. 5B and Fig. 7). In *Cryptococcus neoformans*, CWI pathway mutants were hypersensitive to FD (Kojima et al., 2006) and it was proposed that increased osmotic pressure in the cells due to the activation of the Hog1 pathway also results in the activation of the CWI to reinforce CW. We could not draw significant conclusions on the sensitivity to FD of our Δ*slt2* due to its growth impairment, but our data suggest that it is also more sensitive (Fig. 3C). However, our Δ*kss1* was undoubtedly more sensitive to FD than the wild-type. This latter finding might be explained by the strong basal induction of the Hog1 pathway in the Δ*kss1* mutant (Fig. 5A) and assuming that the activation of this pathway is the main contributor to FD susceptibility. Therefore, our data point to the involvement of the three MAPK pathways, and not only Hog1, in the sensitivity of filamentous fungi to FD, although the elucidation of the specific interactions and roles of Slt2 and Kss1 require further investigation.

AfpB is a class B AFP identified in the genome of *P. digitatum* with potent *in vitro* activity against the self-fungus and other filamentous fungi, and that controls fungal infection *in vivo* (Garrigues et al., 2017b; Garrigues et al., 2018). AfpB has structural and sequence similarities with other class A AFPs such as

583 the AFP from *Aspergillus giganteus* (Martínez del Pozo et al., 2002) or the PAF
584 from *Penicillium chrysogenum* (Hegedüs and Marx, 2013), or with the recently
585 identified class B protein PAFB from *P. chrysogenum* (Huber et al., 2018). The
586 biological role of fungal AFPs for the producer fungus is mostly unknown and
587 the mechanistic studies on their antifungal activity have not yet resulted in a
588 detailed model for their mode of antifungal action, which might also differ among
589 different AFPs (Hegedüs and Marx, 2013; Viragh et al., 2015; Meyer and Jung,
590 2018).

591 There are indications of the involvement of the MAPK pathways in the activity of
592 short antifungal peptides or CRPs including the AFP from *A. giganteus*, the PAF
593 from *P. chrysogenum* or plant defensins (Hayes et al., 2014). The available
594 studies are mostly restricted to yeasts, and in most cases show the involvement
595 of the HOG and/or CWI pathways and the hypersensitivity of the corresponding
596 yeast mutants, as in the examples of the peptidic drugs caspofungin and
597 histatin 5 (Reinoso-Martin et al., 2003; Vylkova et al., 2007) or the plant
598 defensins RsAFP2 (Thevissen et al., 2012) and NaD1 (Hayes et al., 2013). In
599 this later study, and contrary to our observations, osmotic stress induced Hog1
600 phosphorylation much more than NaD1, and Δ*hog1* mutants were more
601 susceptible to defensins. In *S. cerevisiae* mutants, it was reported that
602 CWI/Mpk1 pathway to a lesser extent, and the calcium/calcineurin signalling
603 pathway to a greater extent, are involved in the antifungal activity of the
604 *A. giganteus* AFP (Ouedraogo et al., 2011).

605 These studies have also been extended to filamentous fungi. The AFP from
606 *A. giganteus* induces the CWI response in *Aspergillus nidulans* and *Aspergillus*

607 *niger* through the coordinated signalling of MpkA/Slt2 and calcium pathways
608 (Hagen et al., 2007; Binder et al., 2011). Moreover, *A. nidulans* null mutants of
609 the MpkA/Slt2 CWI MAPK are more sensitive to the AFP from *A. giganteus* or
610 the PAF from *P. chrysogenum* (Binder et al., 2010; Binder et al., 2011). This
611 occurs despite the fact that PAF did not increase the phosphorylation of MpkA
612 (Binder et al., 2010). These previous observations on PAF are contradictory
613 with our study on AfpB, in terms of sensitivity of mutants and induction of Slt2
614 (Fig. 6). Previous reports underline similar discrepancies in the case of different
615 plant defensins and therefore indirectly support our differential findings. Two
616 different plant defensins from *Medicago*, MsDef1 and MtDef4, show substantial
617 differences in their interaction with *F. graminearum* (Ramamoorthy et al., 2007);
618 mutants of Mgv1/Slt2 and Gpmk1/Kss1 are more susceptible to MsDef1, but not
619 to MtDef4. Consistently, both MAPKs are strongly phosphorylated upon
620 treatment with MsDef1 and not with MtDef4. A differential behaviour also occurs
621 in MAPK mutants of *F. oxysporum* that display differences in their response to
622 the defensins NaD1 and NaD2 from *Nicotiana* (Dracatos et al., 2016); Δ*hog1*
623 and Δ*kss1* are more susceptible to NaD1, while Δ*hog1* and Δ*slt2* mutants are
624 more susceptible to NaD2. Hence, the Hog1 pathway is the only conserved
625 response between these two related plant defensins, which is a different pattern
626 from that observed in MsDef1. The synthetic hexapeptide PAF104, which
627 blocks appressorium formation in *M. oryzae,* affects the gene expression of the
628 morphogenetic Pmk1/Kss1 pathway (Rebollar and López-García, 2013).
629 Therefore, there is considerable variation in previous studies on the role of
630 MAPKs in the action of different antifungal peptides and proteins, but the
631 general view is that MAPK mutants, if affected, are more sensitive, which

implies a role in a defence mechanism against proteins/peptides. Our study adds substantial evidence in two different aspects. Firstly, the protein under study (AfpB) is a self-protein identified in the target fungus (*P. digitatum*), and therefore the data can provide information that is relevant to its biological function. Secondly, none of the three MAPK mutants are negatively affected in their sensitivity to AfpB (Fig. 6), similarly to MtDef4 (Ramamoorthy et al., 2007), but are more tolerant at least in the case of Δ*hog1* and Δ*slt2*. These results together with the parallelism in the kinetics of Hog1/Slt2 induction between FD and AfpB (Fig. 5 and 6), points to an active role of the Hog1/Slt2 pathways in the mode of action of AfpB but not in the defence response of *P. digitatum* against the protein.

5. Conclusions

In summary, we conducted a comparative study that demonstrated that the three MAPKs Hog1, Kss1 and Slt2 of the postharvest citrus pathogen *P. digitatum* have differential roles in growth, stress and virulence. Comparatively, the Δ*slt2* mutant showed a strong reduction of growth and conidiation and abnormal morphology, while Δ*kss1* showed a slight growth reduction and Δ*hog1* was the least affected. Both Δ*slt2* and Δ*kss1* mutants showed a strong reduction of virulence, and none of the three mutants sporulated during infection. The analysis of signalling by Hog1 and Slt2 phosphorylation revealed a complex crosstalk that involves the three MAPK pathways. The self-antifungal protein AfpB and the fungicide FD induce the phosphorylation of Hog1 and Slt2, and the analyses of the corresponding mutants revealed the involvement of these MAPKs in their mode of action. The

fact that none of the three MAPK mutants showed increased sensitivity to AfpB but rather higher tolerance indicates that the AfpB-mediated activation of MAPKs would not have a defensive role. Future studies will try to (i) further characterise the mode of action of AfpB in the context of the complex interplay among the MAPK pathways, (ii) determine whether these conclusions hold when AfpB is used against other fungi, and (iii) develop novel control combined treatments with AfpB that reduce the use of fungicides such as FD.

Acknowledgements

This work was funded by BIO2015-68790-C2-1-R project from MINECO/FEDER. We acknowledge critical comments by Dr. Maria Coca (CRAG, Spain), the help in the microscopy experiments of José M. Coll-Marqués (IATA, Spain), and help in the Western assays of Dr. Francisca Rández and Dr. José A. Prieto (IATA, Spain). SG received a predoctoral scholarship (FPU13/04584) from MECD (Spain). We thank Tania Campos and Mª Carmen Molina for their excellent technical assistance.

671 **Figure legends**

672 **Fig. 1.** Growth of *P. digitatum* MAPK mutants and complemented strain in
673 culture. (A) Images of PDA plates after 6 days of growth (top), or minimal
674 medium (PdMMA) plates after 10 days of growth (bottom). (B) Colony diameter
675 on PDA plates from 3 to 9 days. (C) Colony diameter in PdMMA plates from 3 to
676 9 days. (D) Growth measured as OD in 5 % PDB liquid medium for 96 h. (E)
677 Growth measured as OD in 90 % CPE orange extract for 96 h. In this study, the
678 strains are colour and symbol-coded as follows: the parental CECT 20796 in
679 black and filled circles; the Δ*hog1* mutants (for instance, PDMG5121) in green
680 and open squares; the Δ*kss1* mutants (PDMG5212) in red and open diamonds;
681 the Δ*slt2* mutants (PDMG5431) in blue and open triangles; and the Δ*slt2*::*slt2*
682 complemented strain PDMG6134 in blue and filled triangles.

683 **Fig. 2.** Conidia production and conidiophore development are affected in the
684 *P. digitatum* Δ*slt2* mutant. (A) Conidia production of parental CECT 20796
685 (black bars), Δ*slt2* mutant PDMG5431 (dotted blue bars) and complemented
686 PDMG6134 (striped blue bars) strains on PDA plates after 5 and 7 days of
687 growth. One factor analysis of variance (ANOVA) and Tukey´s honestly
688 significant difference (HSD) test at $p < 0.05$ were applied to evaluate statistical
689 significance (indicated by different letters) (SPSS v22.0, SPSS Inc., Chicago, IL,
690 USA). (B-C) Bright field (BF) and fluorescence (CFW) microscopy images of
691 CFW-stained mycelium of the parental CECT 20796, Δ*slt2* mutant
692 (PDMG5431), and the complemented strain (PDMG6134) as indicated.
693 Conidiophores (c) or morphologically altered balloon-structures (b) are

694 indicated. Samples were grown in liquid PDB for 48h (B) or 72h (C). Scale black
695 bars in BF images are 10 µm.

696 **Fig. 3.** Growth of *P. digitatum* MAPK mutants is differentially affected under
697 distinct treatments, stress conditions and fungicides. (A) Effect on growth in
698 PDA (control) supplemented with either 0.5 M NaCl or 1.2 M sorbitol as
699 indicated at the top. Strains in each panel are: parental CECT 20796, Δ*hog1*
700 strains PDMG5121 and PDMG5135, and the ectopic strain PDMG5131 from the
701 same ATMT experiment (top panels); parental CECT 20796, Δ*kss1* strains
702 PDMG5212 and PDMG5241, and the ectopic PDMG5213 (middle panels);
703 parental CECT 20796, Δ*slt2* strains PDMG5422 and PDMG5431, and the
704 ectopic PDMG5412 (bottom panels). (B) Effect on growth in PDA (control)
705 supplemented with 150 µg mL^{-1} CFW, or PDA at 28 ºC. Strains are: parental
706 CECT 20796, the Δ*slt2* mutant PDMG5431 and the Δ*slt2*::*slt2* complemented
707 PDMG6134. (C) Effect on growth in PDA (control) supplemented with either
708 0.4 µg mL^{-1} FD or 2 µg mL^{-1} IPD as indicated at the top. Strains analyzed are:
709 the parental CECT 20796, Δ*hog1* PDMG5121, Δ*kss1* PDMG5212, Δ*slt2*
710 PDMG5431 and complemented Δ*slt2*::*slt2* PDMG6134. In all panels, three ten-
711 fold dilutions of conidia (10^5 to 10^3 conidia mL^{-1}) of strains were inoculated to
712 the wells. The asterisk (*) indicates an error during inoculation; this well was
713 mistakenly omitted and should grow like the parental strain.

714 **Fig. 4.** Differential virulence of *P. digitatum* MAPK mutants to citrus fruits. (A)
715 Percentage of infected wounds in orange fruits inoculated with different
716 *P. digitatum* strains at 5 x 10^4 conidia mL^{-1}. (B) Percentage of infected wounds
717 in mandarin fruits inoculated with different *P. digitatum* strains at the same

718 conidia concentration as in (A). The data indicate the percentage of infected
719 and sporulated wounds (mean value ± SD) at each day post-inoculation (dpi).
720 Representative photographs of orange (C) and mandarin fruits (D) infected with
721 the strains at 7 dpi. (E) Detailed images of necrotic symptoms caused by the
722 Δ*slt2* mutant PDMG5431 in mandarin fruits at 10 dpi. Colours and symbols as
723 indicated in Figure 1.

724 **Fig. 5.** Phosphorylation of *P. digitatum* MAPKs in mutants and in response to
725 different treatments. (A) Phosphorylation of Hog1 and Slt2 in MAPK mutants
726 and parental strain. Note that the P-Hog1 signal and the P-Slt2 signal
727 disappeared in the Δ*hog1* PDMG5121 and in the Δ*slt2* PDMG5431 mutants,
728 respectively. The P-Slt2 signal is recovered in the PDMG6134 complemented
729 strain. (B) Phosphorylation of Hog1 and Slt2 in parental strain CECT 20796
730 treated by H_2O, NaCl, CFW, CR or FD for 20 or 60 min, at the same
731 concentrations as in Figure 3. In (A) and (B) the anti P-p38 (top panels), P-
732 p42/44 (middle) and actin (bottom) antibodies were used on replicates of
733 transferred membranes; the P-Hog1, P-Slt2 and actin signals are labelled with
734 black, white and grey triangles, respectively; and actin was used as loading
735 control. (C-D) Graphs showing the relative quantification of the Western blots of
736 parts (A) and (B), respectively. Relative quantification by densitometry of P-
737 Hog1 and P-Slt2 bands normalised to the actin control and expressed relative to
738 parental levels. n.d. not detected band.

739 **Fig. 6.** Involvement of MAPKs in response of *P. digitatum* to the antifungal
740 protein AfpB. (A) Phosphorylation of Hog1 and Slt2 in wild-type CECT 20796 in
741 response to 10 μg mL^{-1} AfpB treatment for 20 or 60 min. (B) Graphs showing
742 the relative quantification of the Western blots of (A). Other details in (A) and (B)

as in Figure 5. (C) Dose-response curves of *P. digitatum* strains exposed to distinct concentrations of AfpB. Curves show mean ± SD OD_{600} of triplicate samples after 72 h of static incubation at 25 ºC. Colours and symbols as in Figure 1. (D) Bright field microscopy images of representative microtiter wells from the experiment shown in (C), after 7 days of growth.

Fig. 7. A model for the interconnections among the different MAPK pathways and responses to stresses in *P. digitatum*. MAPK colour codes are the same as in the rest of Figures. Stresses are coloured as follows: the CW stress in blue (as the CWI pathway MAPK Slt2), the osmotic stress in green (as the HOG pathway MAPK Hog1), the FD treatment in orange, and the AfpB treatment in purple. Thickness of the lines indicates intensity of response as determined by immunodetection. Arrows indicate induction and bars repression. Asterisks (in green, red, and blue) indicate that the corresponding mutants (Hog1, Kss1, and Slt2) have altered sensitivity to that stress condition.

Supplemental Material.

Supplemental Figure 1. Construction of *P. digitatum* Δ*kss1* strains and verification by PCR analysis.

Supplemental Figure 2. Construction of *P. digitatum* Δ*slt2* strains and verification by PCR analysis.

Supplemental Figure 3. Construction of complementation pCnptII vector.

Supplemental Figure 4. Western blot analyses of phosphorylation levels of MAPK proteins in distinct mutants and in response to different treatments.

Supplemental Figure 5. Phylogenetic relationships of fungal MAPKs.

Supplemental Figure 6. Growth of *P. digitatum* strains in PDA, in PDA supplemented with different compounds and in PDA at different temperatures.

Supplemental Figure 7. Growth of P. digitatum strains in presence of fungicides thiabendazole (TBZ) and imazalil (IMZ).

Supplemental Table 1. PCR primers used to generate and verify the disruption and complementation mutants of *P. digitatum.*

References

Alonso-Monge, R., Carvaihlo, S., Nombela, C., Rial, E., Pla, J., 2009. The Hog1 MAP kinase controls respiratory metabolism in the fungal pathogen *Candida albicans*. Microbiology 155**,** 413-423.

Ballester, A.-R., Lafuente, M.T., Forment, J., Gadea, J., De Vos, R.C.H., Bovy, A.G., GonzÁLez-Candelas, L., 2011. Transcriptomic profiling of citrus fruit peel tissues reveals fundamental effects of phenylpropanoids and ethylene on induced resistance. Mol. Plant Pathol. 12**,** 879-897.

Binder, U., Bencina, M., Eigentler, A., Meyer, V., Marx, F., 2011. The *Aspergillus giganteus* antifungal protein AFP_{NN5353} activates the cell wall integrity pathway and perturbs calcium homeostasis. BMC Microbiol. 11**,** 209.

Binder, U., Oberparleiter, C., Meyer, V., Marx, F., 2010. The antifungal protein PAF interferes with PKC/MPK and cAMP/PKA signalling of *Aspergillus nidulans*. Mol. Microbiol. 75**,** 294-307.

de Ramón-Carbonell, M., Sánchez-Torres, P., 2017. PdSlt2 *Penicillium digitatum* mitogen-activated-protein kinase controls sporulation and virulence during citrus fruit infection. Fungal Biol. 121**,** 1063-1074.

Di Pietro, A., Garcia-Maceira, F.I., Meglecz, E., Roncero, M.I.G., 2001. A MAP kinase of the vascular wilt fungus *Fusarium oxysporum* is essential for root penetration and pathogenesis. Mol. Microbiol. 39**,** 1140-1152.

Dixon, K.P., Xu, J.R., Smirnoff, N., Talbot, N.J., 1999. Independent signaling pathways regulate cellular turgor during hyperosmotic stress and appressorium-mediated plant infection by *Magnaporthe grisea*. Plant Cell 11**,** 2045-58.

Dracatos, P.M., Payne, J., Di Pietro, A., Anderson, M.A., Plummer, K.M., 2016. Plant defensins NaD1 and NaD2 induce different stress response pathways in fungi. Int J Mol Sci 17**,** 1473.

Gandía, M., Harries, E., Marcos, J.F., 2014. The myosin motor domain-containing chitin synthase PdChsVII is required for development, cell wall integrity and virulence in the citrus postharvest pathogen *Penicillium digitatum*. Fungal Genet. Biol. 67**,** 58-70.

García-Rodriguez, L.J., Durán, A., Roncero, C., 2000. Calcofluor antifungal action depends on chitin and a functional high-osmolarity glycerol response (HOG) pathway: Evidence for a physiological role of the *Saccharomyces cerevisiae* HOG pathway under noninducing conditions. J. Bacteriol. 182**,** 2428-2437.

Garrigues, S., Gandía, M., Borics, A., Marx, F., Manzanares, P., Marcos, J.F., 2017a. Mapping and identification of antifungal peptides in the putative

antifungal protein AfpB from the filamentous fungus *Penicillium digitatum*. Front. Microbiol. 8**,** 592.

Garrigues, S., Gandía, M., Castillo, L., Coca, M., Marx, F., Marcos, J.F., Manzanares, P., 2018. Three antifungal proteins from *Penicillium expansum*: Different patterns of production and antifungal activity. Front. Microbiol. 9**,** 2370.

Garrigues, S., Gandía, M., Marcos, J., 2016. Occurrence and function of fungal antifungal proteins: a case study of the citrus postharvest pathogen *Penicillium digitatum*. Appl. Microbiol. Biotechnol. 100**,** 2243-2256.

Garrigues, S., Gandía, M., Popa, C., Borics, A., Marx, F., Coca, M., Marcos, J.F., Manzanares, P., 2017b. Efficient production and characterization of the novel and highly active antifungal protein AfpB from *Penicillium digitatum*. Sci. Rep. 7**,** 14663.

González-Candelas, L., Alamar, S., Sánchez-Torres, P., Zacarías, L., Marcos, J.F., 2010. A transcriptomic approach highlights induction of secondary metabolism in citrus fruit in response to *Penicillium digitatum* infection. BMC Plant Biol. 10**,** 194.

Hagen, S., Marx, F., Ram, A.F., Meyer, V., 2007. The antifungal protein AFP from *Aspergillus giganteus* inhibits chitin synthesis in sensitive fungi. Appl. Environ. Microbiol. 73**,** 2128-2134.

Hamel, L.P., Nicole, M.C., Duplessis, S., Ellis, B.E., 2012. Mitogen-activated protein kinase signaling in plant-interacting fungi: Distinct messages from conserved messengers. Plant Cell 24**,** 1327-1351.

Harries, E., Gandía, M., Carmona, L., Marcos, J.F., 2015. The *Penicillium digitatum* protein O–Mannosyltransferase Pmt2 is required for cell wall integrity, conidiogenesis, virulence and sensitivity to the antifungal peptide PAF26. Mol. Plant Pathol. 16**,** 748-761.

Hayes, B.M., Bleackley, M.R., Wiltshire, J.L., Anderson, M.A., Traven, A., van der Weerden, N.L., 2013. Identification and mechanism of action of the plant defensin NaD1 as a new member of the antifungal drug arsenal against *Candida albicans*. Antimicrob Agents Chemother 57**,** 3667-75.

Hayes, B.M.E., Anderson, M.A., Traven, A., van der Weerden, N.L., Bleackley, M.R., 2014. Activation of stress signalling pathways enhances tolerance of fungi to chemical fungicides and antifungal proteins. Cell. Mol. Life Sci. 71**,** 2651-2666.

He, P., Wang, Y., Wang, X., Zhang, X., Tian, C., 2017. The Mitogen-Activated Protein Kinase *CgMK1* Governs Appressorium Formation, Melanin Synthesis, and Plant Infection of *Colletotrichum gloeosporioides*. Front. Microbiol. 8**,** 2216.

Hegedüs, N., Marx, F., 2013. Antifungal proteins: More than antimicrobials? Fungal Biol. Rev. 26**,** 132-145.

Hernanz-Koers, M., Gandía, M., Garrigues, S., Manzanares, P., Yenush, L., Orzaez, D., Marcos, J.F., 2018. FungalBraid: A GoldenBraid-based modular cloning platform for the assembly and exchange of DNA elements tailored to fungal synthetic biology. Fungal Genet. Biol. 116**,** 51-61.

Huber, A., Hajdu, D., Bratschun-Khan, D., Gaspari, Z., Varbanov, M., Philippot, S., Fizil, A., Czajlik, A., Kele, Z., Sonderegger, C., Galgoczy, L., Bodor, A., Marx, F., Batta, G., 2018. New antimicrobial potential and structural properties of PAFB: A cationic, cysteine-rich protein from *Penicillium chrysogenum* Q176. Sci. Rep. 8**,** 1751.

Jiang, C., Zhang, X., Liu, H., Xu, J.R., 2018. Mitogen-activated protein kinase signaling in plant pathogenic fungi. PLoS Pathog. 14**,** e1006875.

Kanetis, L., Förster, H., Jones, C.A., Borkovich, K.A., Adaskaveg, J.E., 2008. Characterization of genetic and biochemical mechanisms of fludioxonil and pyrimethanil resistance in field isolates of *Penicillium digitatum*. Phytopathology 98**,** 205-214.

Khang, C.H., Park, S.Y., Rho, H.S., Lee, Y.H., Kang, S., 2006. Filamentous fungi (*Magnaporthe grisea* and *Fusarium oxysporum*). Meth. Mol. Biol. 344**,** 403-420.

Kojima, K., Bahn, Y.-S., Heitman, J., 2006. Calcineurin, Mpk1 and Hog1 MAPK pathways independently control fludioxonil antifungal sensitivity in *Cryptococcus neoformans*. Microbiology 152**,** 591-604.

Liu, J., Tong, S.-M., Qiu, L., Ying, S.-H., Feng, M.-G., 2017. Two histidine kinases can sense different stress cues for activation of the MAPK Hog1 in a fungal insect pathogen. Environ. Microbiol. 19**,** 4091-4102.

Liu, W., Leroux, P., Fillinger, S., 2008. The HOG1-like MAP kinase Sak1 of *Botrytis cinerea* is negatively regulated by the upstream histidine kinase Bos1 and is not involved in dicarboximide- and phenylpyrrole-resistance. Fungal Genet. Biol. 45**,** 1062-1074.

López-García, B., Pérez-Payá, E., Marcos, J.F., 2002. Identification of novel hexapeptides bioactive against phytopathogenic fungi through screening of a synthetic peptide combinatorial library. Appl. Environ. Microbiol. 68**,** 2453-2460.

López-Pérez, M., Ballester, A.-R., González-Candelas, L., 2015. Identification and functional analysis of *Penicillium digitatum* genes putatively involved in virulence towards citrus fruit. Mol. Plant Pathol. 16**,** 262-275.

Luo, X., Keyhani, N.O., Yu, X., He, Z., Luo, Z., Pei, Y., Zhang, Y., 2012. The MAP kinase Bbslt2 controls growth, conidiation, cell wall integrity, and virulence in the insect pathogenic fungus *Beauveria bassiana*. Fungal Genet. Biol. 49**,** 544-555.

Ma, H., Sun, X., Wang, M., Gai, Y., Chung, K.-R., Li, H., 2016. The citrus postharvest pathogen *Penicillium digitatum* depends on the PdMpkB kinase for developmental and virulence functions. Int. J. Food Microbiol. 236, 167-176.

Marcet-Houben, M., Ballester, A.R., de la Fuente, B., Harries, E., Marcos, J.F., González-Candelas, L., Gabaldón, T., 2012. Genome sequence of the necrotrophic fungus *Penicillium digitatum*, the main postharvest pathogen of citrus. BMC Genomics 13, 646.

Marcos, J.F., Muñoz, A., Pérez-Payá, E., Misra, S., López-García, B., 2008. Identification and rational design of novel antimicrobial peptides for plant protection. Annu. Rev. Phytopathol. 46, 273-301.

Martínez del Pozo, A., Lacadena, V., Mancheño, J.M., Olmo, N., Oñaderra, M., Gavilanes, J.G., 2002. The antifungal protein AFP of Aspergillus giganteus is an oligonucleotide/oligosaccharide binding (OB) fold-containing protein that produces condensation of DNA. J. Biol. Chem. 277, 46179-46183.

Mehrabi, R., M'Barek, S.B., Saidi, A., Abrinbana, M., De Wit, P.J.G.M., Kema, G.H.J., MAP kinase phosphorylation and cAMP assessment in fungi. Meth. Mol. Biol., Vol. 835, 2012, pp. 571-583.

Meyer, V., 2008. A small protein that fights fungi: AFP as a new promising antifungal agent of biotechnological value. Appl. Microbiol. Biotech. 78, 17-28.

Meyer, V., Jung, S., 2018. Antifungal Peptides of the AFP Family Revisited: Are These Cannibal Toxins? Microorganisms 6, 50.

Motoyama, T., Ochiai, N., Morita, M., Iida, Y., Usami, R., Kudo, T., 2008. Involvement of putative response regulator genes of the rice blast fungus *Magnaporthe oryzae* in osmotic stress response, fungicide action, and pathogenicity. Curr. Genet. 54, 185.

Munro, C.A., Selvaggini, S., De Bruijn, I., Walker, L., Lenardon, M.D., Gerssen, B., Milne, S., Brown, A.J.P., Gow, N.A.R., 2007. The PKC, HOG and Ca2+ signalling pathways co-ordinately regulate chitin synthesis in *Candida albicans*. Mol. Microbiol. 63, 1399-1413.

Nguyen, T.V., Schäfer, W., Bormann, J., 2012. The Stress-Activated Protein Kinase FgOS-2 Is a Key Regulator in the Life Cycle of the Cereal Pathogen *Fusarium graminearum*. Mol. Plant-Microbe Interact. 25, 1142-1156.

Ouedraogo, J.P., Hagen, S., Spielvogel, A., Engelhardt, S., Meyer, V., 2011. Survival strategies of yeast and filamentous fungi against the antifungal protein AFP. J. Biol. Chem. 286, 13859-13868.

935 Palou, L., *Penicillium digitatum*, *Penicillium italicum* (Green Mold, Blue Mold), in:
936 Bautista-Baños, S., (Eds.), Postharvest Decay: Control Strategies, 2014,
937 pp. 45-102.

938 Palou, L., Ali, A., Fallik, E., Romanazzi, G., 2016. GRAS, plant- and animal-
939 derived compounds as alternatives to conventional fungicides for the
940 control of postharvest diseases of fresh horticultural produce.
941 Postharvest Biol. Tec. 122**,** 41-52.

942 Pareek, M., Rajam, M.V., 2017. RNAi-mediated silencing of MAP kinase
943 signalling genes (*Fmk1*, *Hog1* and *Pbs2*) in *Fusarium oxysporum*
944 reduces pathogenesis on tomato plants. Fungal Biol. 121**,** 775-784.

945 Pillonel, C., Meyer, T., 1997. Effect of phenylpyrroles on glycerol accumulation
946 and protein kinase activity of *Neurospora crassa*. Pesticide Science 49**,**
947 229-236.

948 Ramamoorthy, V., Zhao, X.H., Snyder, A.K., Xu, J.R., Shah, D.M., 2007. Two
949 mitogen-activated protein kinase signalling cascades mediate basal
950 resistance to antifungal plant defensins in *Fusarium graminearum*. Cell.
951 Microbiol. 9**,** 1491-1506.

952 Rebollar, A., López-García, B., 2013. PAF104, a synthetic peptide to control
953 rice blast disease by blocking appressorium formation in *Magnaporthe*
954 *oryzae*. Mol. Plant-Microbe Interact. 26**,** 1407-1416.

955 Reinoso-Martin, C., Schuller, C., Schuetzer-Muehlbauer, M., Kuchler, K., 2003.
956 The yeast protein kinase C cell integrity pathway mediates tolerance to
957 the antifungal drug caspofungin through activation of Slt2p mitogen-
958 activated protein kinase signaling. Eukaryot. Cell 2**,** 1200-1210.

959 Rispail, N., Soanes, D.M., Ant, C., Czajkowski, R., Grunler, A., Huguet, R.,
960 Perez-Nadales, E., Poli, A., Sartorel, E., Valiante, V., Yang, M., Beffa, R.,
961 Brakhage, A.A., Gow, N.A.R., Kahmann, R., Lebrun, M.H., Lenasi, H.,
962 Perez-Martin, J., Talbot, N.J., Wendland, J., Di Pietro, A., 2009.
963 Comparative genomics of MAP kinase and calcium-calcineurin signalling
964 components in plant and human pathogenic fungi. Fungal Genet. Biol.
965 46**,** 287-298.

966 Rodríguez-Peña, J.M., Pérez-Díaz, R.M., Alvarez, S., Bermejo, C., García, R.,
967 Santiago, C., Nombela, C., Arroyo, J., 2005. The 'yeast cell wall chip' - A
968 tool to analyse the regulation of cell wall biogenesis in Saccharomyces
969 cerevisiae. Microbiology 151**,** 2241-2249.

970 Roman, E., Arana, D.M., Nombela, C., Alonso-Monge, R., Pla, J., 2007. MAP
971 kinase pathways as regulators of fungal virulence. Trends Microbiol 15**,**
972 181-90.

973 Rui, O., Hahn, M., 2007. The Slt2-type MAP kinase Bmp3 of *Botrytis cinerea* is
974 required for normal saprotrophic growth, conidiation, plant surface
975 sensing and host tissue colonization. Mol. Plant Pathol. 8**,** 173-184.

976 Sakulkoo, W., Osés-Ruiz, M., Oliveira Garcia, E., Soanes, D.M., Littlejohn,
977 G.R., Hacker, C., Correia, A., Valent, B., Talbot, N.J., 2018. A single
978 fungal MAP kinase controls plant cell-to-cell invasion by the rice blast
979 fungus. Science 359**,** 1399-1403.

980 Schindelin, J., Arganda-Carreras, I., Frise, E., Kaynig, V., Longair, M., Pietzsch,
981 T., Preibisch, S., Rueden, C., Saalfeld, S., Schmid, B., Tinevez, J.Y.,
982 White, D.J., Hartenstein, V., Eliceiri, K., Tomancak, P., Cardona, A.,
983 2012. Fiji: an open-source platform for biological-image analysis. Nat.
984 Methods 9**,** 676-82.

985 Segmuller, N., Ellendorf, U., Tudzynski, B., Tudzynski, P., 2007. BcSAK1, a
986 stress-activated mitogen-activated protein kinase, is involved in
987 vegetative differentiation and pathogenicity in *Botrytis cinerea*. Eukaryot.
988 Cell 6**,** 211-221.

989 Segorbe, D., Di Pietro, A., Pérez-Nadales, E., Turrà, D., 2016. Three *Fusarium*
990 *oxysporum* MAPKs have distinct and complementary roles in stress
991 adaptation and cross-kingdom pathogenicity. Mol. Plant Pathol. 18**,** 912-
992 924.

993 Shi, X., Cordero, T., Garrigues, S., Marcos, J.F., Daròs, J.-A., Coca, M., 2019.
994 Efficient production of antifungal proteins in plants using a new transient
995 expression vector derived from tobacco mosaic virus. Plant Biotechnol. J.
996 doi:10.1111/pbi.13038.

997 Siewers, V., Viaud, M., Jimenez-Teja, D., Collado, I.G., Schulze Gronover, C.,
998 Pradier, J.M., Tudzynsk, B., Tudzynski, P., 2005. Functional analysis of
999 the cytochrome P450 monooxygenase gene *bcbot1* of *Botrytis cinerea*
1000 indicates that botrydial is a strain-specific virulence factor. Mol. Plant-
1001 Microbe Interact. 18**,** 602-612.

1002 Sonderegger, C., Galgóczy, L., Garrigues, S., Fizil, Á., Borics, A., Manzanares,
1003 P., Hegedüs, N., Huber, A., Marcos, J.F., Batta, G., Marx, F., 2016. A
1004 *Penicillium chrysogenum*-based expression system for the production of
1005 small, cysteine-rich antifungal proteins for structural and functional
1006 analyses. Microb. Cell Fact. 15**,** 192.

1007 Song, Z., Zhong, Q., Yin, Y., Shen, L., Li, Y., Wang, Z., 2016. The high osmotic
1008 response and cell wall integrity pathways cooperate to regulate
1009 morphology, microsclerotia development, and virulence in *Metarhizium*
1010 *rileyi*. Sci. Rep. 6**,** 38765.

1011 Sun, X., Ruan, R., Lin, L., Zhu, C., Zhang, T., Wang, M., Li, H., Yu, D., 2013.
1012 Genomewide investigation into DNA elements and ABC transporters
1013 involved in imazalil resistance in *Penicillium digitatum*. FEMS Microbiol.
1014 Lett. 348**,** 11-18.

1015 Takano, Y., Kikuchi, T., Kubo, Y., Hamer, J.E., Mise, K., Furusawa, I., 2000.
1016 The Colletotrichum lagenarium MAP kinase gene CMK1 regulates

diverse aspects of fungal pathogenesis. Mol. Plant-Microbe Interact. 13**,** 374-383.

Thevissen, K., de Mello Tavares, P., Xu, D., Blankenship, J., Vandenbosch, D., Idkowiak-Baldys, J., Govaert, G., Bink, A., Rozental, S., de Groot, P.W.J., Davis, T.R., Kumamoto, C.A., Vargas, G., Nimrichter, L., Coenye, T., Mitchell, A., Roemer, T., Hannun, Y.A., Cammue, B.P.A., 2012. The plant defensin RsAFP2 induces cell wall stress, septin mislocalization and accumulation of ceramides in *Candida albicans*. Mol. Microbiol. 84**,** 166-180.

Torres-Quiroz, F., Garcia-Marques, S., Coria, R., Randez-Gil, F., Prieto, J.A., 2010. The activity of yeast Hog1 MAPK is required during endoplasmic reticulum stress induced by tunicamycin exposure. J. Biol. Chem. 285**,** 20088-96.

Turrà, D., Segorbe, D., Di Pietro, A., 2014. Protein kinases in plant-pathogenic Fungi: Conserved regulators of infection. Annu. Rev. Phytopathol. 52**,** 267-288.

Vilanova, L., Teixidó, N., Torres, R., Usall, J., Viñas, I., Sánchez-Torres, P., 2016. Relevance of the transcription factor *PdSte12* in *Penicillium digitatum* conidiation and virulence during citrus fruit infection. Int. J. Food Microbiol. 235**,** 93-102.

Viragh, M., Marton, A., Vizler, C., Toth, L., Vagvolgyi, C., Marx, F., Galgoczy, L., 2015. Insight into the antifungal mechanism of *Neosartorya fischeri* antifungal protein. Prot Cell 6**,** 518-28.

Vylkova, S., Jang, W.S., Li, W.S., Nayyar, N., Edgerton, M., 2007. Histatin 5 initiates osmotic stress response in *Candida albicans* via activation of the Hog1 mitogen-activated protein kinase pathway. Eukaryot. Cell 6**,** 1876-1888.

Wang, M., Chen, C., Zhu, C., Sun, X., Ruan, R., Li, H., 2014. *Os2* MAP kinase-mediated osmostress tolerance in *Penicillium digitatum* is associated with its positive regulation on glycerol synthesis and negative regulation on ergosterol synthesis. Microbiol. Res. 169**,** 511-521.

Wang, M., Sun, X., Zhu, C., Xu, Q., Ruan, R., Yu, D., Li, H., 2015. *PdbrlA*, *PdabaA* and *PdwetA* control distinct stages of conidiogenesis in *Penicillium digitatum*. Res. Microbiol. 166**,** 56-65.

Yang, Q., Jiang, J., Mayr, C., Hahn, M., Ma, Z., 2013. Involvement of two type 2C protein phosphatases BcPtc1 and BcPtc3 in the regulation of multiple stress tolerance and virulence of *Botrytis cinerea*. Environ. Microbiol.

Zhang, X., Liu, W., Li, Y., Li, G., Xu, J.R., 2017. Expression of HopAI interferes with MAP kinase signalling in *Magnaporthe oryzae*. Environ. Microbiol. 19**,** 4190-4204.

Zhang, Y., Lamm, R., Pillonel, C., Lam, S., Xu, J.R., 2002. Osmoregulation and fungicide resistance: the *Neurospora crassa os-2* gene encodes a HOG1 mitogen-activated protein kinase homologue. Appl. Environ. Microbiol. 68**,** 532-538.

Zheng, D., Zhang, S., Zhou, X., Wang, C., Xiang, P., Zheng, Q., Xu, J.R., 2012. The FgHOG1 pathway regulates hyphal growth, stress responses, and plant infection in *Fusarium graminearum*. PLoS ONE 7**,** e49495.

Zheng, L., Campbell, M., Murphy, J., Lam, S., Xu, J.R., 2000. The *BMP1* gene is essential for pathogenicity in the gray mold fungus *Botrytis cinerea*. Mol. Plant-Microbe Interact. 13**,** 724-32.

Figure 1 (Gandía et al., 2018)

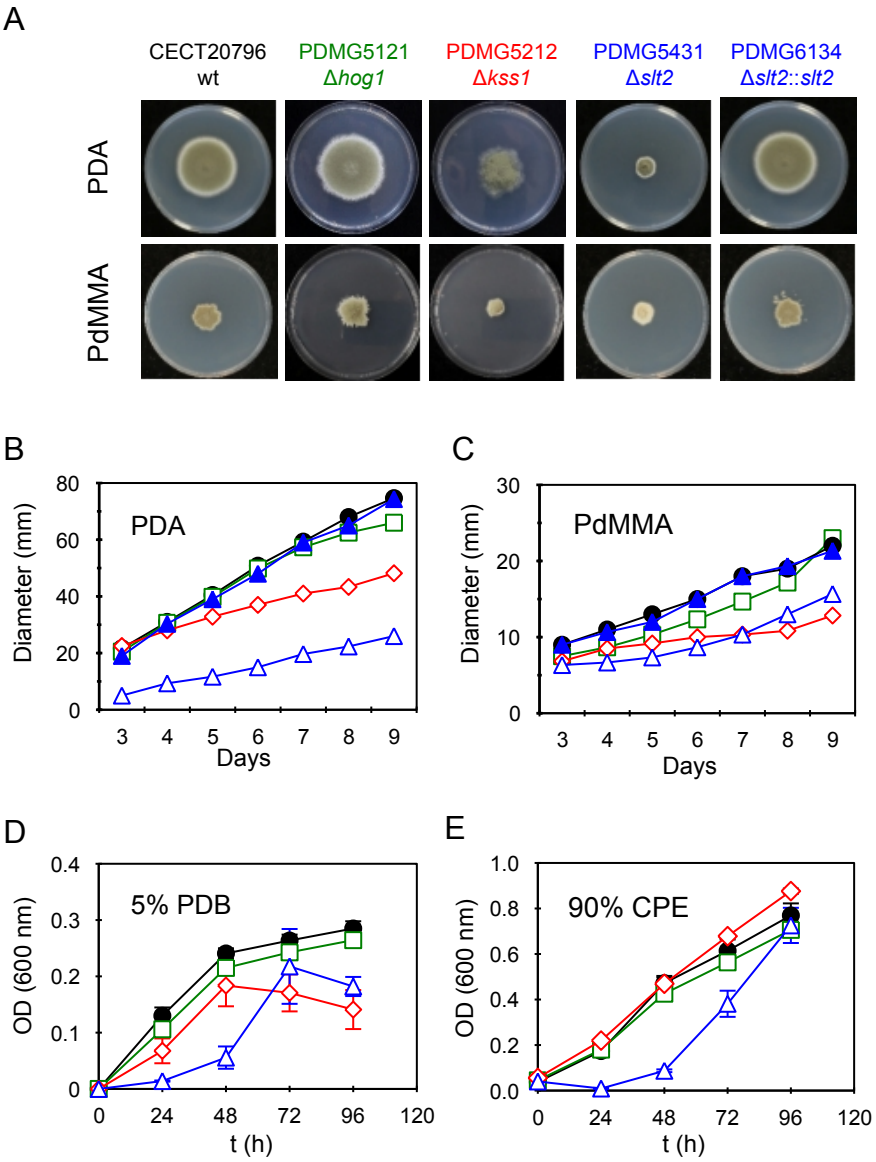

Figure 2 (Gandía et al., 2018)

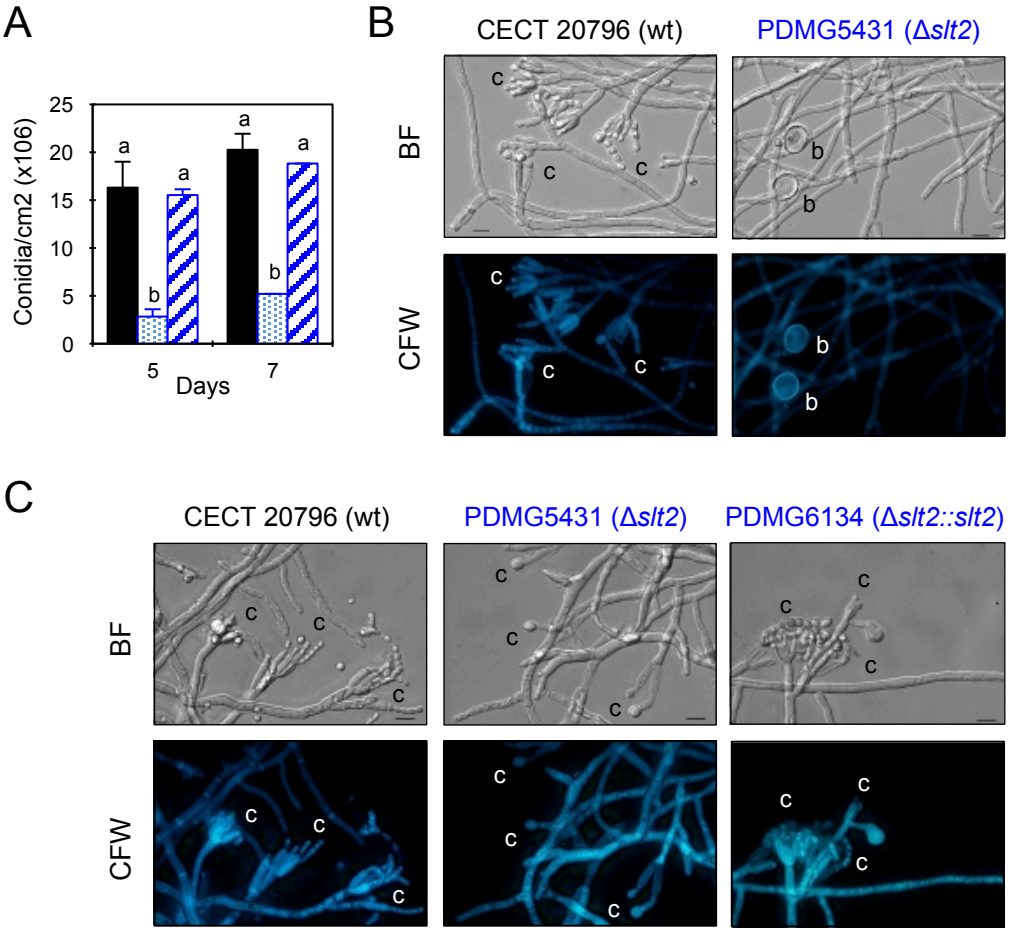

Figure 3 (Gandía et al., 2018)

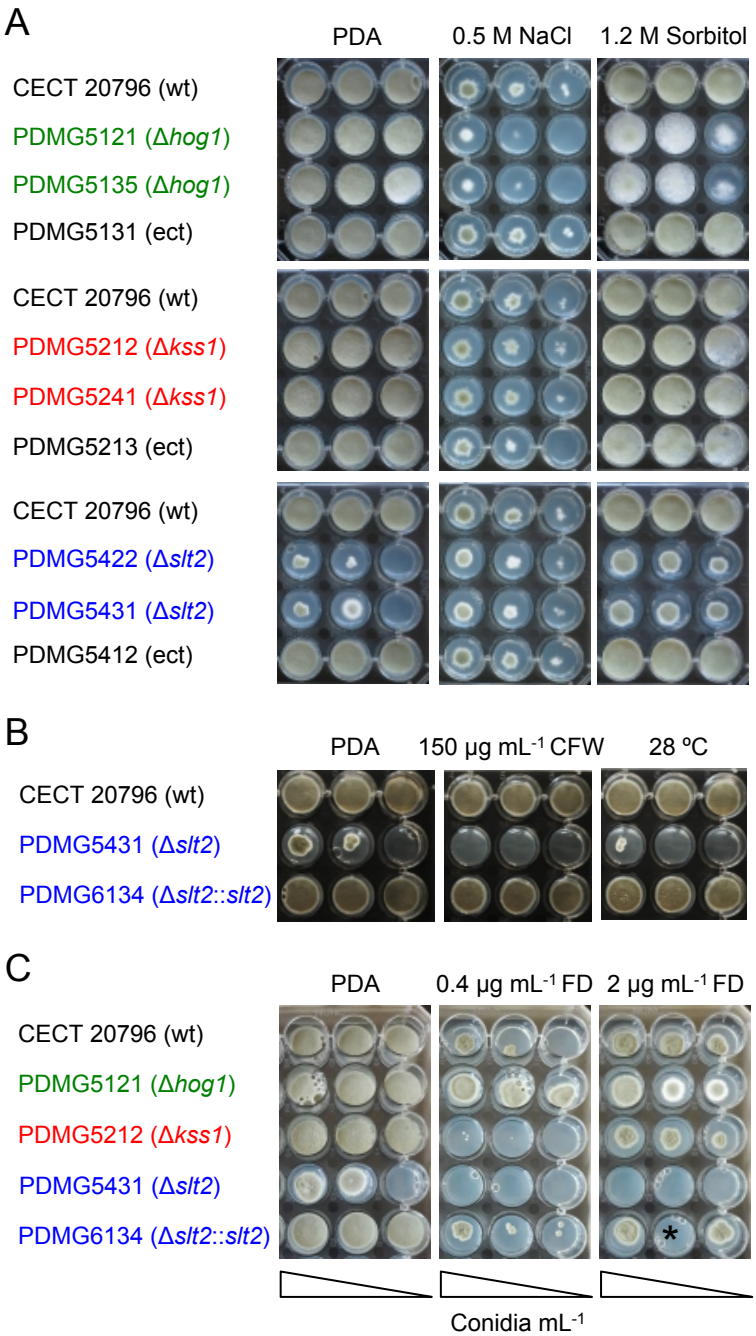

Figure 4 (Gandía et al., 2018)

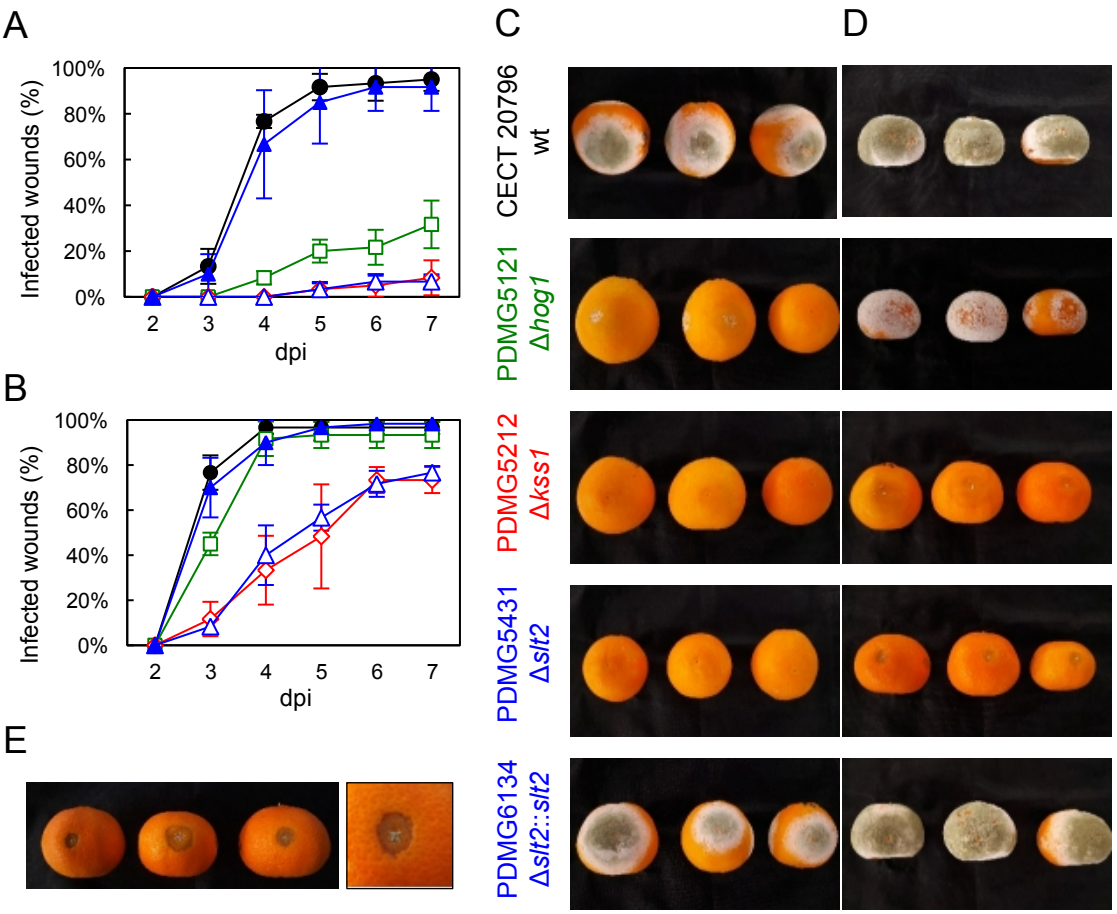

Figure 5 (Gandía et al., 2018)

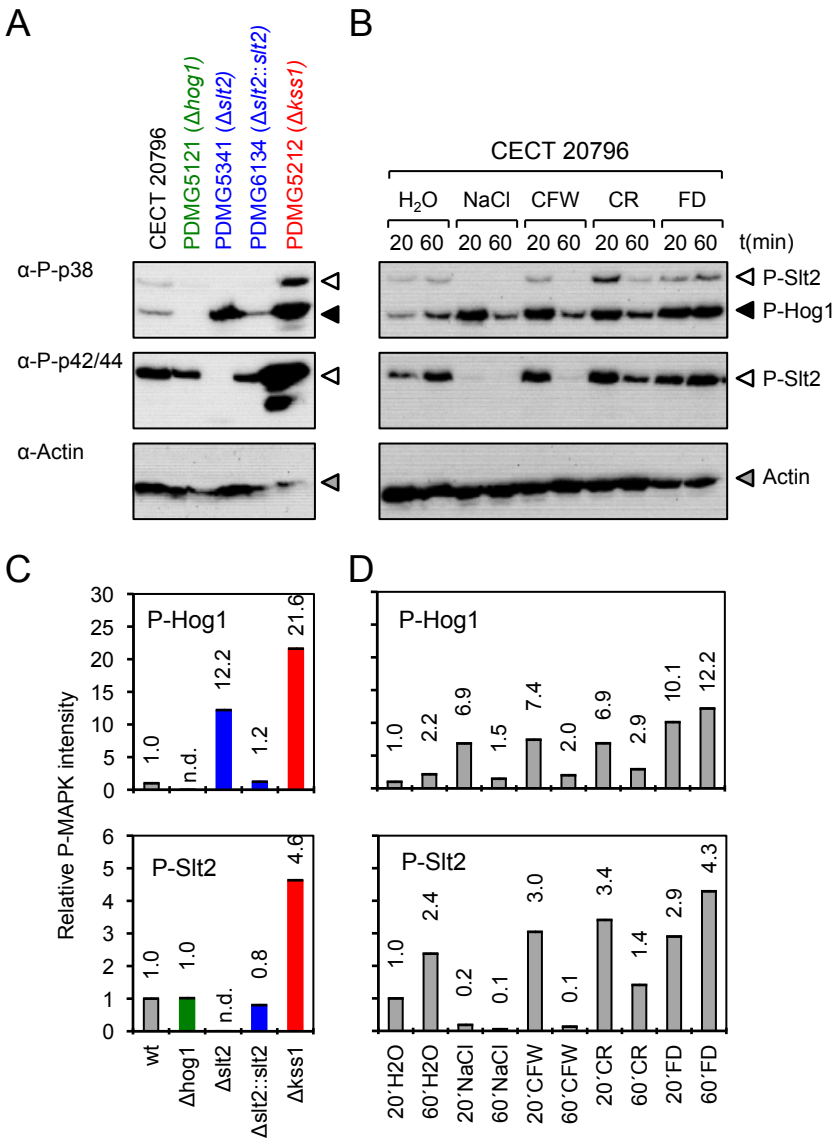

Figure 6 (Gandía et al., 2018)

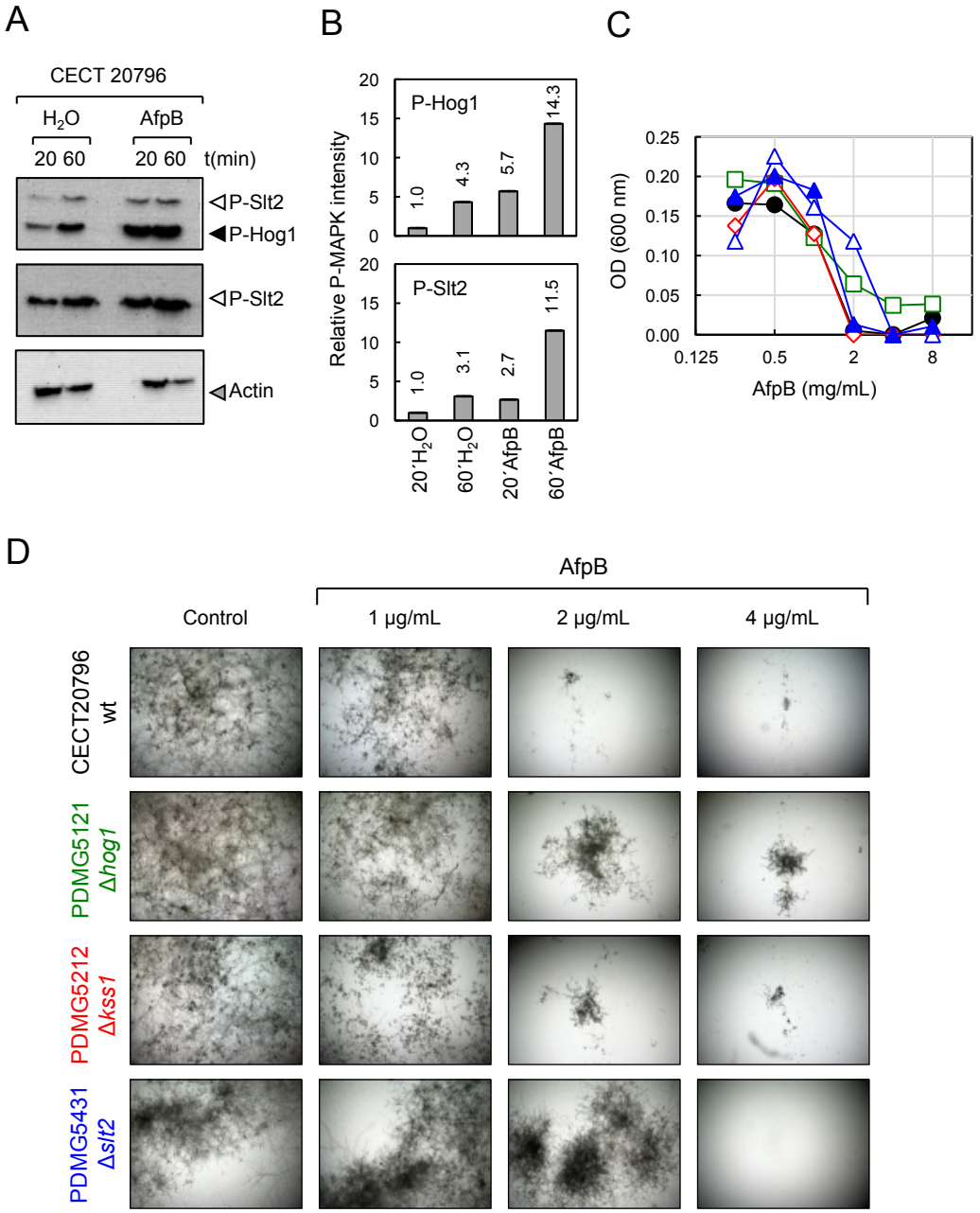

Figure 7 (Gandía et al., 2018)

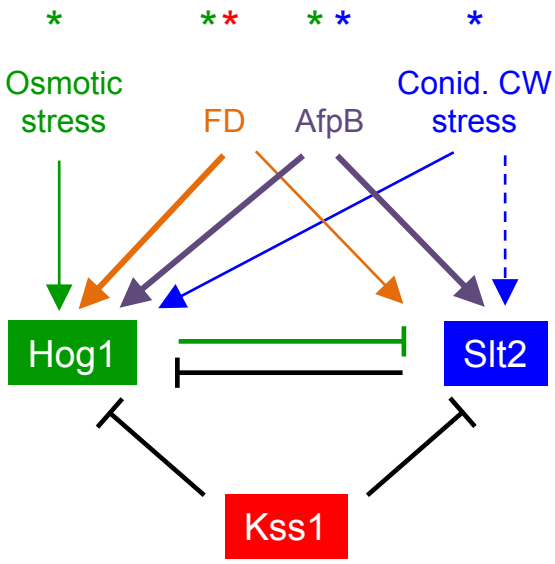

Supplemental Table 1. PCR primers used to generate and verify the disruption and complementation mutants of *Penicillium digitatum*.

Primer	Location	Gene	Sequence 5´- 3´	Use*	Strain**	Reference
OJM197	5´	P*trpC*	CGTTAACTGATATTGAAGGAGCAT	F	KO/EC/C	Gandía et al., 2014
OJM232	Intern	*hph*	GTTTGCCAGTGATACACATGGG	R	KO/EC/C	Gandía et al., 2014
OJM311	5´	HSV*tk*	CCACGGAAGTCCGCCCGGAGC	F	EC	Gandía et al., 2014
OJM312	3´	HSV*tk*	GACGTGCATGGAACGGAGGCG	R	EC	Gandía et al., 2014
OJM518	3´	*nptII*	GCGC**CGTCTC**GCTCAAAGCTCAGAAGAACTCGTCAAGAAG	R	C	Hernanz-Koers et al., 2018
OJM533	5´	pDGB3α2	CGAGTGGTGATTTTGTGCCG	F	-----	Hernanz-Koers et al., 2018
OJM534	3´	pDGB3α2	CCCGCCAATATATCCTGTCAG	R	-----	Hernanz-Koers et al., 2018
OJM543	5´	*Pdkss1*	GCGC**CGTCTC**GCTCGTACTCCGCCTTTAGCATATACTGAA	F	-----	This work
OJM544	5´	*Pdkss1*	GCGC**CGTCTC**GCTCACATTTAAGAACGTGGTATGTTAGTGG	R	-----	This work
OJM545	3´	*Pdkss1*	GCGC**CGTCTC**GCTCGGCTTCAATACTTCATCTATCAGACCC	F	-----	This work
OJM546	3´	*Pdkss1*	GCGC**CGTCTC**GCTCAAGCGAAAGGGCAGTGTAGGGTTTG	R	-----	This work
OJM551	5´	*Pdslt2*	GCGC**CGTCTC**GCTCGTACTAACACGAACGGAATTCAATAAGAT	F	-----	This work

OJM552	5´	*Pdslt2*	GCGC**CGTCTC**GCTCACATTCTACATTGCGATGGCCACGG	R	-----	This work
OJM553	3´	*Pdslt2*	GCGC**CGTCTC**GCTCGGCTTACTGCCCCACGACCTTCGAT	F	-----	This work
OJM554	3´	*Pdslt2*	GCGC**CGTCTC**GCTCAAGCGTTAACTTAGAGATAGAGGCATTGA	R	-----	This work
OJM555	3´	T*tub*	TCATCATGCAACATGCATGTA	R	KO/EC/C	Hernanz-Koers et al., 2018
OJM562	5´	*Pdkss1*	GCCCTGTCTTCTACTCACGGACC	F	wt/KO	This work
OJM565	5´	*Pdkss1*	GAAGGAGATCTTTCGGGATCCTCC	R	wt/EC	This work
OJM570	5´	*Pdslt2*	CGGATCTGTCCGATCTCAGGG	F	wt/KO/C	This work
OJM571	3´	*Pdslt2*	CGAGTCCCGTTGTCTGGAAACCC	R	wt/KO/C	This work
OJM574	5´	*Pdslt2*	CGTCTAGACCCGGGGACAAGATAGGGCTGG	F	KO/C	This work
OJM575	3´	*Pdslt2*	TTTCTAGAAGCTTACAAAAGTCACATCAAAGG	R	KO/C	This work

*F: Forward; R: Reverse. **wt: wild type; KO: null mutant; EC: Ectopic transformant; C: Complementation strain. *Bsm*BI restriction sites are in bold

Supplemental Figure 1 (Gandía et al., 2018)

A

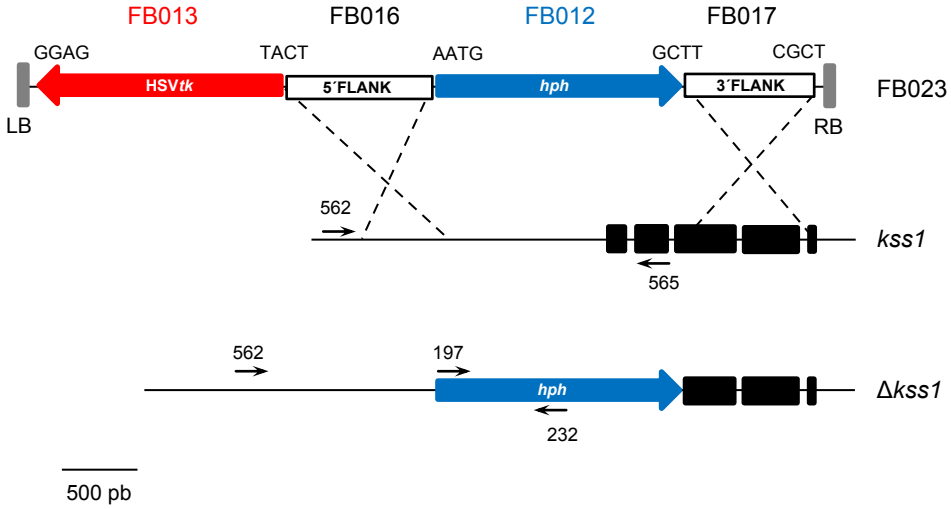

B

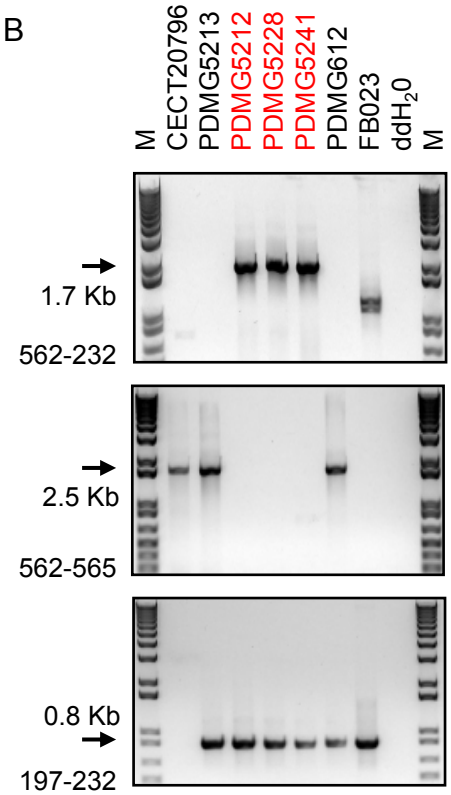

Supplemental Figure 1: Construction of *P. digitatum* Δ*kss1* strains and verification by PCR analysis.

(A) Schematic diagram of constructions for gene replacement. The binary vector FB023 (pDGB3α2 backbone) designed for *kss1* gene disruption containing positive (*hph*) and negative (HSV*tk*) selection markers (top) indicating the 4-nucleotide DNA barcodes used to assemble different plasmids (adapted from Hernanz-Koers et al., 2018), the *kss1* gene in parental strain CECT 20796 (middle), the Δ*kss1* disrupted gene obtained (bottom). All primers used for PCR analysis are localized in the figure.

(B) PCR amplification of genomic DNA of the different *P. digitatum* strains with different primer pairs as indicated. The disruption mutants (in red) showed the same amplicon (1.7 Kb) with primers OJM562/OJM232 located outside gene replacement construction and inside hygromycin resistant marker respectively. On the other hand, CECT 20796 wild type strain, ectopic strains (PDMG5213 obtained in this transformation assay and PDMG612 obtained in a previous assay) and FB023 vector, not shown any amplicon with these primers (top panel). Using primers OJM562/OJM565 located (respectively) outside gene replacement construction and inside *kss1* gene replaced by hygromycin marker, only CECT 20796 strain and ectopic transformants showed an expected amplicon of 2.5 Kb (middle panel). All the transformants and FB023 vector gave a positive band with specific hygromycin primers OJM197/OJM232 indicating the presence of this marker (bottom panel).

Supplemental Figure 2 (Gandía et al., 2018)

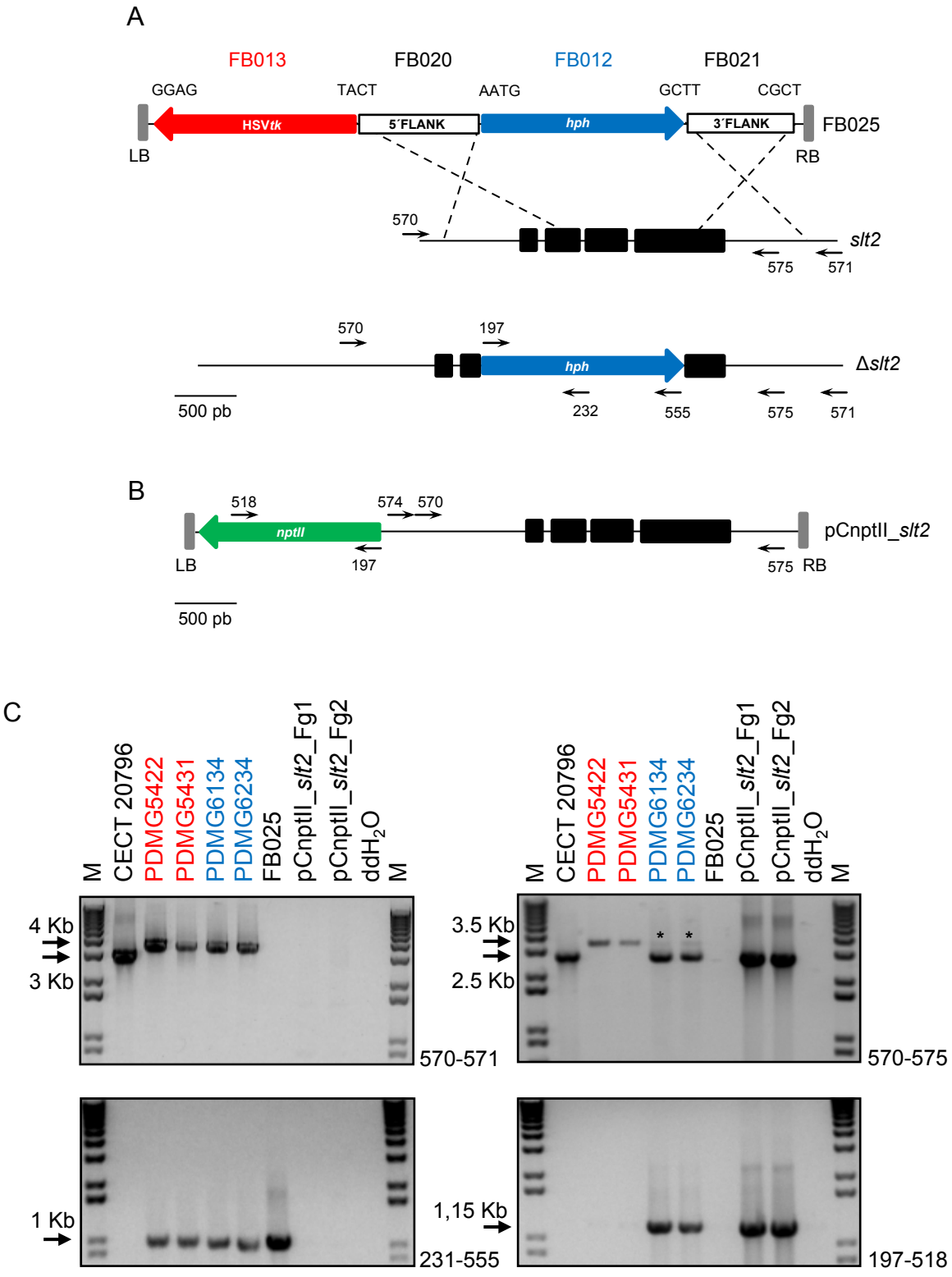

Supplemental Figure 2: Construction of *P. digitatum* Δ*slt2* strains and verification by PCR analysis.

(A) Schematic diagram of different constructions for gene replacement. The binary vector FB025 (pDGB3α2 backbone) designed for *slt2* gene disruption containing positive (*hph*) and negative (HSV*tk*) selection markers (top) indicating the 4-nucleotide DNA barcodes used to assemble different plasmids (adapted from Hernanz-Koers et al., 2018), the *slt2* gene in parental strain CECT 20796 (second draw), the Δ*slt2* disrupted gene obtained (third draw). All primers used for PCR analysis are localized in the figure.

(B) Schematic diagram of complementation construction containing *nptII* gene which confers resistance to geneticin. All primers used for PCR analysis are localized in the figure.

(C) Amplification

pairs as indicated. The disruption mutants PDMG5422 and PDMG5431 (in red) together with complementation strains PDMG6134 and PDMG6234 (in blue) showed the same amplicon either (4 Kb) with primers OJM570/OJM571 located outside gene replacement construction, while CECT 20796 wild type strain showed a PCR fragment with different size (3 Kb) (left top panel). Using primers OJM570/OJM575 different amplicon size was determined among CECT 20796 strain (2.5 Kb) and PDMG5422 and PDMG5431 mutants (3.5 Kb), while complementation mutants PDMG6134 and PDMG6234 showed both amplification fragments as expected (amplicon as mutant strains marked by an asterisk; right top panel). All the transformants and FB025 vector gave a positive band with primers OJM231/OJM555 indicating the presence of the hygromycin marker (left bottom panel). On the other hand, only complementación mutants PDMG6134 and PDMG6234 and two independent vectors generated to complementation strategy, showed the presence of *nptII* marker with primers OJM197/OJM518 as expected (right bottom panel).

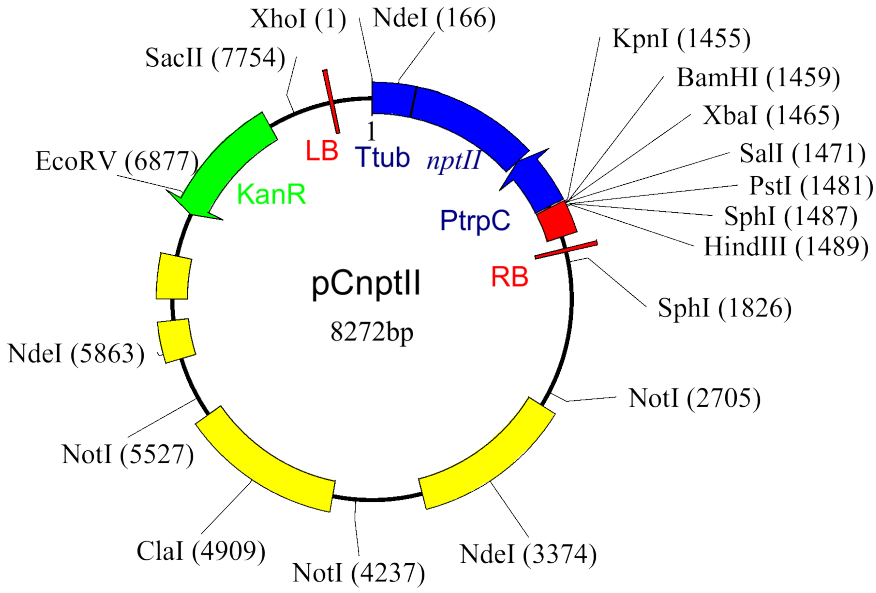

Supplemental Figure 3. Construction of complementation pCnptII vector. Schematic restriction map of pCnptII vector using for complementation. pCnptII was constructed from pCAMBIA_1300 substituting the *hph* selection marker for hygromicin by the positive selection marker *nptII* for kanamycin/G418 resistance from *E. coli,* under the regulation of the promoter P*trpC* from *A. nidulans* and the T*tub* terminator from *N. crassa*.

Supplemental Figure 4 (Gandía et al., 2018)

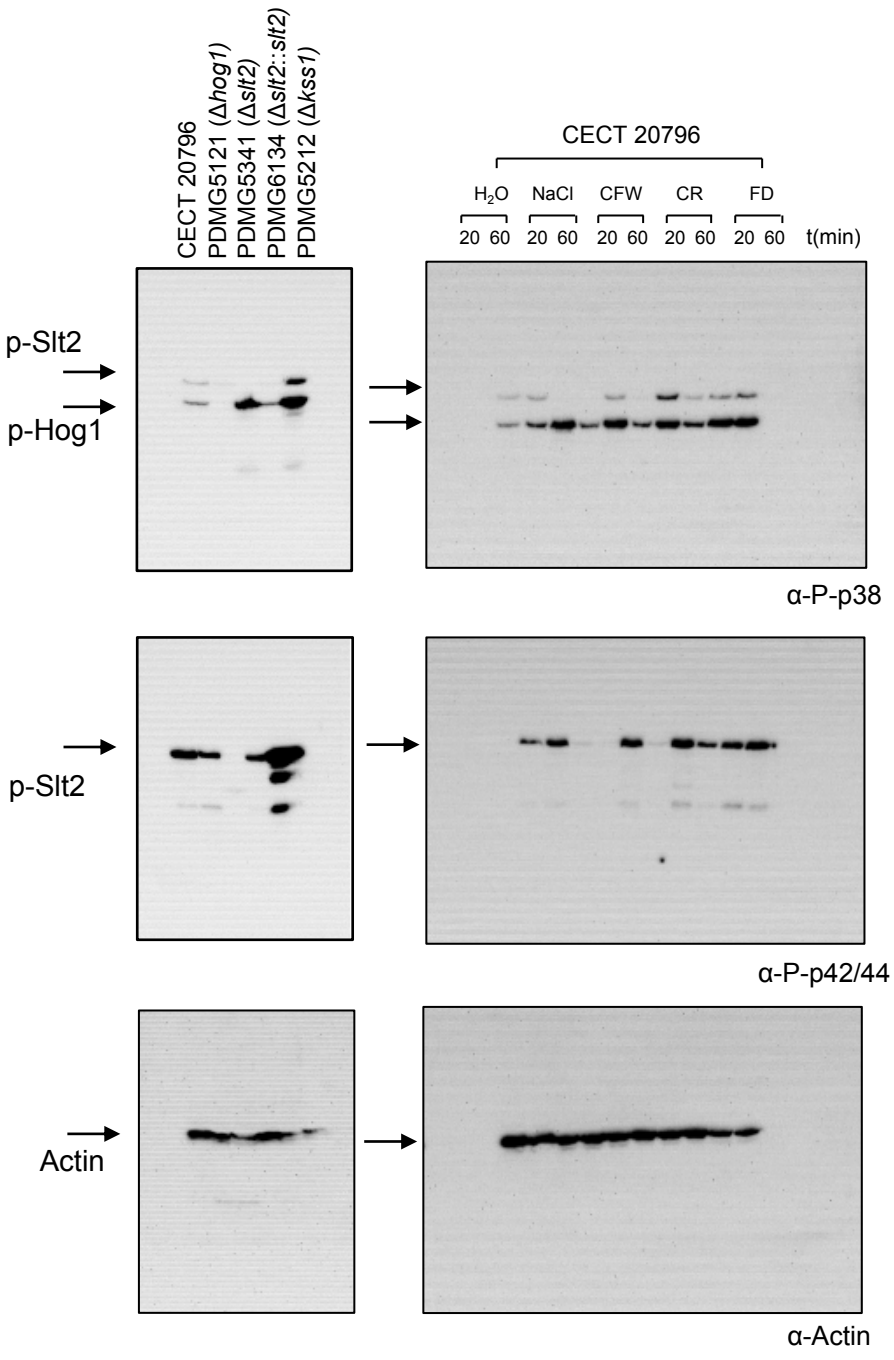

Supplemental Figure 4: Western blot analyses of phosphorylation levels of MAPK proteins in distinct mutants and in response to different treatments .
Complete membrane hybridization of western blot analyses shown in Figure 6

Supplemental Figure 5 (Gandía et al., 2018)

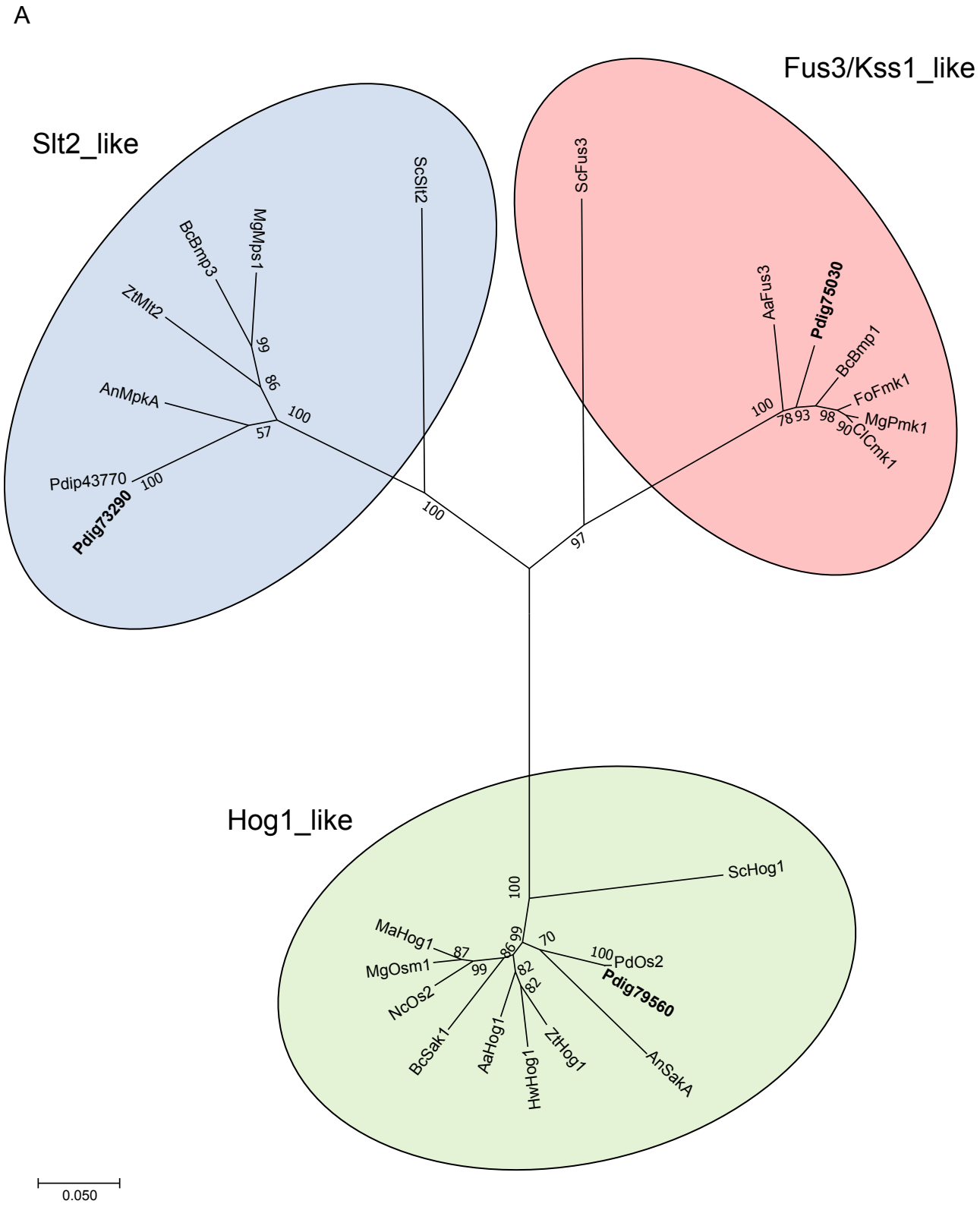

B

Fungus	Gene	Accession Number (NCBI/UniProt)
Penicillium digitatum	*Pdig_73290*	EKV07468/K9FXQ2
	Pdip_43770	EKV14402/K9G0Q2
	Pdig_75030	EKV07229/K9FDB7
	PdOs2	HQ416719/E5LCJ8
	Pdig_79560	EKV06178/K9FTS6
Alternaria alternata	*Fus3*	ACY73851/D2IV71
	Hog1	GQ414509/D3J126
Aspergillus nidulans	*MpkA*	CBF81444/C8VFS8
	Hog1/SakA	AAF97243/Q9P419
Botrytis cinerea	*Bmp3*	ABJ51957/Q000T6
	Bmp1	AAG23132/Q9HG08
	Hog1/Sak1	AM236311/A1IVT7
Colletotrichum lagenarium	*Cmk1*	AAD50496/Q9UW09
Fusarium oxysporum	*Fmk1*	AAG01162/Q9HGU2
Hortaea werneckii	*Hog1*	AF516914/Q8NJT7
Magnaporthe grisea	*Mps1*	AAC63682/O13352
	Pmk1	AAC49521/Q92246
	Hog1/Osm1	AAF09475/Q9UV51
Metarhizium acridum	*Hog1*	EFY85878/E9EDY6
Neurospora crassa	*Hog1/Os2*	AF297031/Q96TL5
Saccharomyces cerevisiae	*Slt2/Mpk1*	CAA41954/Q00772
	Fus3	AAA34613/P16892
	Hog1	AAA34680/P32485
Zymoseptoria tritici	*Mlt2*	AAY98511/Q1G7H6
	Hog1	DQ432031/Q1KTF2

Supplemental Figure 5. Phylogenetic relationships of fungal MAPKs.

(A) Neighbor-Joining tree of MAPK from different fungi obtained with MEGA7. The optimal tree with the sum of branch length = 2.06236153 is shown. The tree is drawn to scale, with branch lengths in the same units as those of the evolutionary distances used to infer it. Bootstrap values of 10,000 replicates are shown at the nodes of each branch. Sequences characterized in this study are in bold. There were a total of 529 positions in the final dataset.

(B) Accession number of sequences used in phylogenetic analyses obtained at the National Center for Biotechnology Information(http://www.ncbi.nlm.nih.gov) and at the UniProt (http://www.uniprot.org) servers.

Supplemental Figure 6 (Gandía et al., 2018)

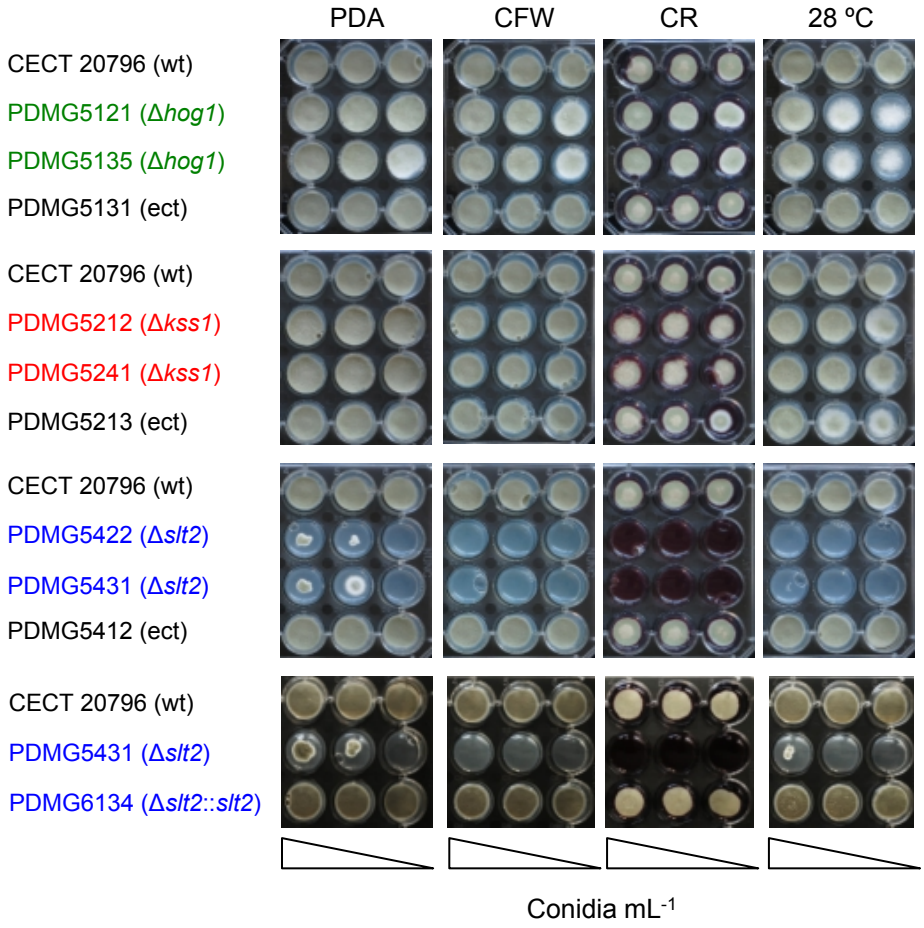

Supplemental Figure 6: Growth of *P. digitatum* strains in PDA, in PDA supplemented with different compounds and in PDA at different temperatures. The strains and experiments shown are the same as in Figure 3. Growth after 4 days at 25 ºC of 10-fold dilution conidia of strains (10^5 to 10^3 conidia mL^{-1}) in PDA medium (control) compared with growth in PDA supplemented with 150 µg mL^{-1} of Calcofluor white (CFW), with 150 µg mL^{-1} of Congo red (CR) and in PDA medium at 28 ºC.

Supplemental Figure 7 (Gandía et al., 2018)

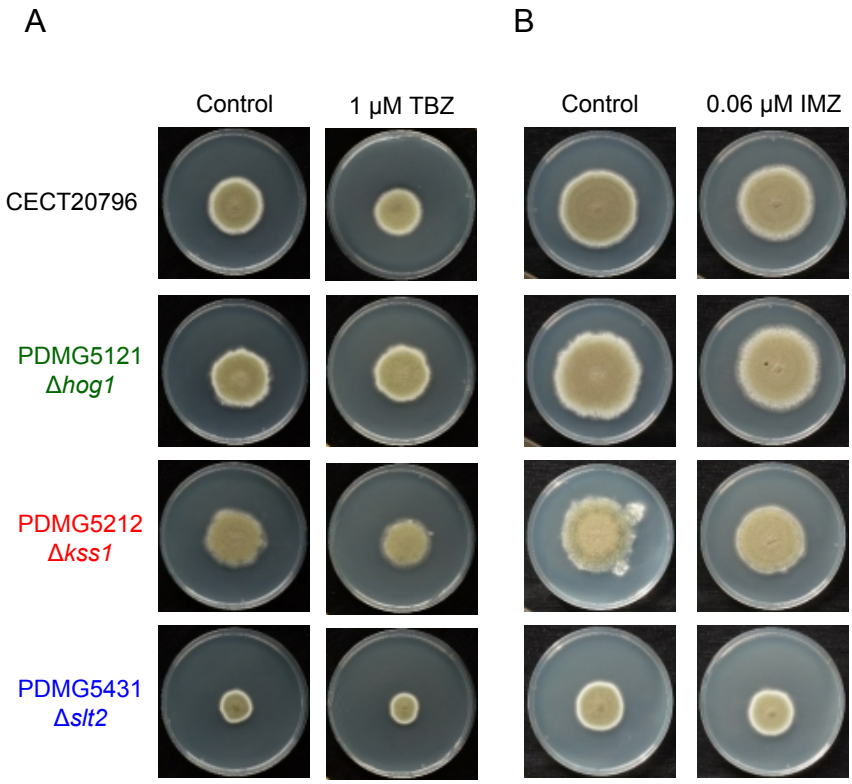

Supplemental Figure 7: Growth of *P. digitatum* strains in presence of fungicides thiabendazol (TBZ) and imazalil (IMZ). Strains shown are: the parental CECT 20796 in black; the Δ*hog1* mutant PDMG5121 in green; the Δ*kss1* mutant PDMG5212 in red; and the Δ*slt2* mutant PDMG5431 in blue. (A) Growth after 5 days at 25 ºC in PDA (control) compared with growth in PDA supplemented with 1 µM TBZ. (B) Growth after 7 days at 25 ºC in PDA (control) compared with growth in PDA supplemented with 0.06 µM IMZ.